Dimensional crossover of nonrelativistic bosons

Soeren Lammers,[1] Igor Boettcher,[2,*] and Christof Wetterich[1]

[1]*Institute for Theoretical Physics, University of Heidelberg, D-69120 Heidelberg, Germany*
[2]*Department of Physics, Simon Fraser University, Burnaby, British Columbia V5A 1S6, Canada*

We investigate how confining a transverse spatial dimension influences the few- and many-body properties of nonrelativistic bosons with pointlike interactions. Our main focus is on the dimensional crossover from three to two dimensions, which is of relevance for ultracold-atom experiments. Using functional-renormalization-group equations and T-matrix calculations we study how the phase transition temperature changes as a function of the spatial extent of the transverse dimension and relate the three- and two-dimensional s-wave scattering lengths. The analysis reveals how the properties of the lower-dimensional system are inherited from the higher-dimensional one during renormalization-group evolution. We limit the discussion to confinements in a potential well with periodic boundary conditions and argue why this qualitatively captures the physics of other compactifications such as transverse harmonic confinement as in cold-atom experiments.

I. INTRODUCTION

Lower-dimensional systems play a prominent role in statistical and condensed matter physics, as they exhibit several unusual features due to the pronounced influence of fluctuations. At the same time, many technologically interesting materials such as high-temperature superconductors and graphene are based on layered or striped crystalline structures and thus inherit some of their properties from the reduced dimensionality. To disentangle the influence of dimensionality effects from other aspects of the many-body system constitutes a key challenge in advancing our understanding of condensed matter and in devising new promising materials.

With the recent progress in trapping ultracold quantum gases it has become feasible to simulate lower-dimensional Hamiltonians by means of atoms in strongly anisotropic external potentials [1,2]. For instance, in two dimensions, the algebraically correlated superfluid and the corresponding Berezinskii-Kosterlitz-Thouless phase transition have been observed for both bosons [3–8] and fermion pairs [9,10]. A characteristic of these types of experiments is that the final setup might, due to an insufficient degree of anisotropy of the trap in comparison to the density of the system, still feature aspects of the three-dimensional (3D) system. This anisotropy may be quantified by the relative spacing of energy levels for excitations related to different spatial directions or by the aspect ratios of trapping frequencies in different directions. For a finite anisotropy ratio, the system is, in general, in a dimensional crossover without a well-defined dimensionality. Whereas this is typically an unwanted effect in the quantum simulation of two-dimensional (2D) and one-dimensional (1D) Hamiltonians, it can also be seen as a possibility to implement new types of quantum matter with interesting properties. The aim of this paper is to investigate the few- and many-body properties of a particularly simple system, the Bose gas with pointlike interactions, in the dimensional crossover.

Consider for simplicity the crossover from three to two dimensions by means of compactifying the "transverse" z direction. However, the following argumentation is not limited to this particular case. As a particularly instructive transverse confinement, we delimit the z direction by a potential well of length L. The boundary conditions at the end points may be chosen periodic, in which case we also say that the system is confined to a torus in the z direction. We may also restrict the system to a box potential with infinitely high walls given by

$$V_{\text{box}}(z) = \begin{cases} 0, & 0 \leqslant z \leqslant L; \\ \infty & \text{otherwise.} \end{cases} \quad (1)$$

In both cases, the trapping potential inside the well vanishes, and thus the confinement reduces to the boundary conditions on the bosonic field $\phi(\tau,\vec{x})$ or, equivalently, the coordinates of the many-body wave function in a first-quantized formulation. These boundary conditions read

$$\phi(\tau,x,y,z=0) = \phi(\tau,x,y,z=L) \quad (2)$$

for periodic boundary conditions (pbc) and

$$\phi(\tau,x,y,z=0) = \phi(\tau,x,y,z=L) = 0 \quad (3)$$

for the box. The boundary conditions lead to a quantization of energies and thus a discrete excitation spectrum in the z direction.

In a functional integral formulation of the many-body quantum system, the boundary conditions appear as restrictions on the appropriate function space. This can be related to energy levels of noninteracting excitations, and eigenstates of the interacting system are not needed for this purpose. In our setting the eigenfunctions in the z direction are superpositions of plane waves with momentum component q_z, and the boundary conditions (2) and (3) lead to a quantization of energies $E_z = \hbar^2 q_z^2/2M$. For the torus we have $q_z \to k_n$ with

$$k_n = \frac{2\pi n}{L}, \quad n \in \mathbb{Z}, \quad (4)$$

whereas in a box we have $E_z \to \hbar^2 \kappa_n^2/(2M)$ with $\kappa_n = \frac{\pi n}{L}$, $n = 1,2,\ldots$. Importantly, the box features a nonvanishing zero-point energy, E_0, whereas a trap with pbc does not. Since realistic confinements such as they appear in cold-atom experiments are implemented by means of smoothly varying
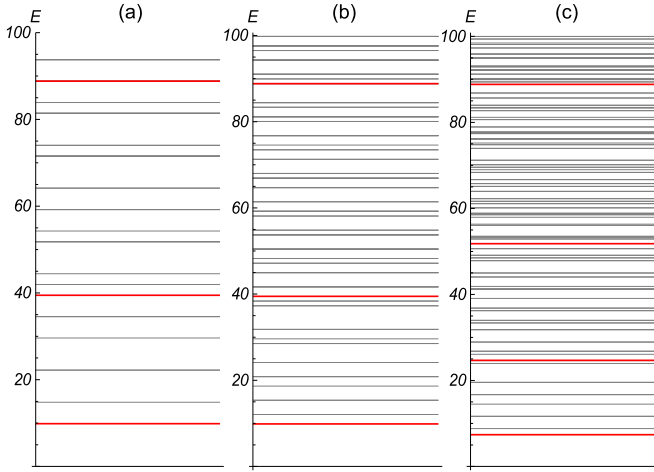
_____

*iboettch@sfu.ca

FIG. 1. Schematics of the energy spectrum in the dimensional crossover from three to two dimensions. (a, b) Discrete eigenenergies for a noninteracting system in a 3D box potential which confines the system to the cuboid $(x,y,z) \in [0,L_x]^2 \times [0,L]$. In (a) we have set $L_x/L = 2$, whereas (b) displays the case of $L_x/L = 3$. As we increase the ratio L_x/L, an effective 2D continuum of states (thin gray lines) fills the region between the discrete spectrum of excitations in the transverse z direction (thick red lines). The lowest excitations appear above the zero-point energy, which is generally not 0. (c) Sketch of the more realistic scenario of a system which is interacting and confined by a smooth trapping potential. Although the concrete mode spectrum and level spacing in (c) differ from those in (a) and (b), we find the same qualitative behavior.

trapping potentials and not potential wells, our analysis can only reveal qualitative statements. For example, in the case of a harmonic trap the function space consists of Hermite functions, again with a discrete energy spectrum. For an increasing anisotropy the level spacing in the x and y directions goes to 0 compared to the one in the z direction. We illustrate these statements in Fig. 1.

In our setting we need to compare L with the length scales associated with many-body physics such as the density and temperature. The regime where L is much smaller than all these length scales is called the 2D limit, because the system will be in its ground state in the z direction and the low-energy excitations are limited to the 2D continuum (q_x, q_y) in momentum space just above the zero-point energy E_0. The 3D system then macroscopically looks like a 2D system. In our analysis below we also address the question how the parameters of the effective 2D system are inherited from the 3D system.

Our formulation bears a great resemblance to other systems where "dimensional reduction" occurs. This concerns, for example, the transition from effective quantum statistics to classical statistics as the temperature T drops below the relevant energy scales of the system. In the Matsubara formalism, $1/T$ plays the same role as L in our case. Another example is the dimensional reduction of higher-dimensional Kaluza-Klein theories compactified on a torus. The main difference from systems in relativistic quantum field theory is the different nonrelativistic dispersion relation in our setting.

This paper is organized as follows. In Sec. II we introduce the Bose gas in the dimensional crossover. In Sec. III we study the superfluid phase transition in the crossover from three to two dimensions by means of the functional renormalization group (FRG). The scattering properties in the 2D limit are studied with the FRG and T-matrix calculations in Sec. IV. In Sec. V we discuss the relevance of our calculations for more realistic confinements and give an outlook on extensions of our approach. In Appendix A1 and A2, we study the behavior of the critical temperature in the 2D limit, and in Appendixes B and C we derive the FRG flow equation in the dimensional crossover in detail and relate the T matrix, scattering vertex, and dimer propagator within the FRG framework.

II. MODEL

We study nonrelativistic bosons with repulsive pointlike interactions. This provides an excellent description of ultracold quantum gases of alkali-metal atoms, where the precise form of interatomic interactions is irrelevant for macroscopic physics and can thus be replaced by a pointlike s-wave coupling constant, λ_Λ, which eventually relates to an experimentally measurable scattering length, a. The model may, however, also be used as an effective description of nonrelativistic bosonic degrees of freedom in other condensed matter setups.

We employ a functional integral formulation with the Euclidean microscopic action of the system given by

$$S[\varphi] = \int_X \left[\varphi^* \left(\partial_\tau - \frac{\nabla^2}{2M} - \mu \right) \varphi + \frac{\lambda_\Lambda}{2} |\varphi|^4 \right]. \quad (5)$$

Herein, the bosonic degrees of freedom are described by the complex scalar field $\varphi = \varphi(\tau, \vec{x})$. We abbreviate $\int_X = \int_0^\beta d\tau \int d^D x$, the number of spatial dimensions is D, and τ denotes imaginary time. The latter is compactified to a torus of circumference $\beta = (k_B T)^{-1}$ with temperature T. The chemical potential and atomic mass are denoted μ and M, respectively. The action is defined with respect to an ultraviolet cutoff Λ, which is of the order of the inverse van der Waals length for ultracold atoms. We use units such that $\hbar = k_B = 2M = 1$.

The few- and many-body properties of the system described by the action, (5), are captured by the partition function of the system. Equivalently, this information is encoded in the effective action or free energy $\Gamma[\phi; \mu, T, \lambda, \Lambda]$, which is a functional of the mean field $\phi(x) = \langle \varphi(x) \rangle$ in the presence of general inhomogeneous sources $J(x)$. In the following we employ the FRG to deduce properties of Γ within approximations. The approach is based on the exact evolution equation for the effective average action Γ_k [11,12] given by

$$\partial_k \Gamma_k = \frac{1}{2} \text{Tr} \left[\left(\Gamma_k^{(2)} + R_k \right)^{-1} \partial_k R_k \right], \quad (6)$$

where k is a momentum scale such that $\Gamma_{k=\Lambda} = S$ for some ultraviolet scale Λ and $\Gamma_{k=0} = \Gamma$ [13–21]. The second functional derivative of Γ is denoted $\Gamma^{(2)}$, and R_k is a regulator function, which can be chosen freely within some limitations [22].

In order to approximate the right-hand side of the flow equation, (6), we apply the ansatz

$$\Gamma_k[\phi] = \int_X [\phi^*(Z_k \partial_\tau - \nabla^2)\phi + U_k(|\phi|^2)] \qquad (7)$$

in the implementation of Refs. [23–25]. Our main interest is in the effective potential U_k, which we evaluate here for a homogeneous field ϕ. This is well suited for pbc, while for the box the field $\phi(z) \sim \sin(\pi z/L)$ should improve the approximation. (In principle, one could include different potentials for several of the low-lying modes in the z direction.) For the present analysis it is sufficient to employ a ϕ^4 expansion for the effective average potential $U_k(\rho)$ according to

$$U_k(\rho) = m_k^2 \rho + \frac{\lambda_k}{2}\rho^2, \qquad (8)$$

with U(1)-invariant $\rho = \phi^*\phi$. In Eq. (7) we use a renormalized field ϕ chosen such that the prefactor of $\phi^*\nabla^2\phi$ is unity. This explains why the expectation value of ϕ can be nonzero even in the 2D limit, where the Mermin-Wagner theorem [26,27] forbids long-range order.

We denote the k-dependent minimum of $U_k(\rho)$ by $\rho_{0,k}$. The normal and superfluid phases of the system are distinguished by means of $\rho_{0,k\to 0}$ being 0 and nonzero, respectively. The ansatz in Eq. (8) has been successfully applied to describe universal and nonuniversal features of the nonrelativistic Bose gas in both three and two dimensions. In particular, the thermodynamic equation of state [28,29], critical exponents [13,30], and critical temperature T_c [25,29] have been obtained in good quantitative agreement with other theoretical approaches [31–34] and with experiment [35–37]. Extension of the ansatz, (8), for Γ_k of the 2D Bose gas have been devised in Refs. [38–40] to capture, for instance, the emergence of Popov's hydrodynamic description at low energies and the essential scaling at the BKT transition.

Given the success of ansatz (8) in providing a qualitatively and mostly quantitatively correct description of the 3D and 2D nonrelativistic Bose gas, it is natural to apply it to the question of the dimensional crossover from three to two dimensions. For spatial dimensions $2 < D \leqslant 3$, the system features long-range order below the critical temperature T_c. For $D = 2$, a superfluid phase with power-law decay of correlations and nonzero superfluid density $\rho_{0,k\to 0}$ exists below a critical temperature T_c [41–44]. Investigating the location of the minimum $\rho_{0,k}$ of the effective average potential in the limit $k \to 0$ thus allows for a unified description of the superfluid transition for all $2 \leqslant D \leqslant 3$.

The derivative expansion employed in Eq. (7) is spatially isotropic in the sense that excitations in the planar and transverse directions are treated equally. More generally, the kinetic energy of excitations may be approximated as

$$E_{\rm kin}(\vec{q},q_z) = \vec{q}^2 + \xi q_z^2, \qquad (9)$$

where $\vec{q}$ is the momentum vector in the plane, and q_z is the component in the transverse (confined) direction. We call this more general ansatz the anisotropic derivative expansion. In Appendix B we show that it reproduces the same results as the ansatz in Eq. (7) with $\xi = 1$, because ξ remains of order unity and is not exceptionally small. Accordingly, excitations in the transverse direction with momentum $q_z \sim L^{-1}$ are still

energetically costly for $L \to 0$ and thus decouple from the low-energy physics. As soon as they are decoupled, however, the precise value of the prefactor ξ is unimportant. A detailed discussion is presented in Appendix B.

It is instructive to study the role of ρ_0 in the dimensional crossover in terms of the effective action. For this consider the 3D effective action ansatz

$$\Gamma[\phi] = \int_X \int_0^L dz \bigg(\phi^*\big(Z_k \partial_\tau - \nabla - \partial_z^2 + m^2\big)\phi + \frac{\lambda_{\rm 3D}}{2}|\phi|^4 \bigg), \qquad (10)$$

where we denote $X = (\tau,\vec{x})$, with $\vec{x} = (x,y)$. The field $\rho = |\phi|^2$ has the physical dimension of a 3D number density. The ground state $\phi_0(\tau,\vec{x},z)$ of the 3D system with $L = \infty$ is given by a constant value ϕ_0 with arbitrary complex phase. The same holds for pbc, where we can write

$$\phi_0^{\rm (pbc)}(\tau,\vec{x},z) = \chi_0 \frac{1}{\sqrt{L}}, \qquad (11)$$

with $|\chi_0|^2$ having the dimension of a 2D number density. The effective action evaluated for this configuration reads

$$\Gamma\big[\phi_0^{\rm (qbc)}\big] = \int_X \bigg(m^2|\chi_0|^2 + \frac{(\lambda_{\rm 3D}/L)}{2}|\chi_0|^4 \bigg). \qquad (12)$$

It resembles the one of a 2D Bose gas with coupling constant $\lambda_{\rm 2D} = \lambda_{\rm 3D}/L$. (Since $\lambda_{\rm 3D}$ has the dimension of a length, $\lambda_{\rm 2D}$ is dimensionless.) For a confinement in a box we have an inhomogeneous ground state given by

$$\phi_0^{\rm (box)}(\tau,z,\vec{x}) = \chi_0 \sqrt{\frac{2}{L}} \sin\left(\frac{\pi z}{L}\right). \qquad (13)$$

For this configuration we have

$$\Gamma\big[\phi_0^{\rm (box)}\big] = \int_X \left[\left(m^2 + \frac{\pi^2}{L^2}\right)|\chi_0|^2 + \frac{\lambda_{\rm 2D}}{2}|\chi_0|^4 \right], \qquad (14)$$

with $\lambda_{\rm 2D} = I_2 \frac{\lambda_{\rm 3D}}{L}$, $I_2 = \frac{4}{L}\int_0^L dz \sin^4(\frac{\pi z}{L}) = \frac{3}{2}$. Hence, for confinement with sharp boundary conditions we find a nontrivial prefactor in the translation between the coupling constants on the mean-field level, namely, $\lambda_{\rm 2D} = 3\lambda_{\rm 3D}/(2L)$. The coherence properties of ultracold Bose gases in the dimensional crossover with confining box potentials have been discussed in Ref. [45].

The FRG approach has been applied to study the effect of compactified dimensions on many-body systems both in several relativistic and in nonrelativistic setups. Finite-volume effects, i.e., when *all* spatial directions are confined to a cube of size $[0,L]^d$, have been studied for quark-meson models [46–49] and the 3D BCS-BEC crossover [50]. In particular, Ref. [49] highlights the difference between periodic and antiperiodic boundary conditions. The latter result in a nonvanishing zero-point energy similar to the confinement in a box potential discussed above. In Sec. V we discuss the role the zero-point energy plays in the FRG setup on the basis of our findings for the dimensional crossover.

III. SUPERFLUID TRANSITION

The flow of the effective average action Γ_k is initialized at some ultraviolet momentum scale $k = \Lambda$, where Γ_Λ coincides with the microscopic action, (5), of a 3D Bose gas. The compactification in the z direction introduces a new scale to the 3D system, which is defined by the size L of the potential well. In particular, note that if L^{-1} is much larger than the many-body scales, the system is effectively two-dimensional. We examine this scenario in Sec. IV. However, the UV scale Λ is always chosen in a way so that $\Lambda \gg (L^{-1}, \mu^{1/2}, T^{1/2})$, i.e., we start with a 3D system with 3D coupling constants. The initial value for the effective potential is given by

$$U_\Lambda(\rho) = \frac{\lambda_\Lambda}{2}(\rho - \rho_{0,\Lambda})^2, \tag{15}$$

with $\rho_{0,\Lambda} = \mu/\lambda_\Lambda$. In practice, we initialize the flow at the UV scale, $\Lambda/\sqrt{\mu} = 10^3$, and stop at the final scale, $k_{\mathrm{f}} = \Lambda e^{-10}$, which is much smaller than the many-body scales.

The flow equation of the effective average potential U_k factorizes into a universal L-independent part $G_1(T)$ and a crossover function $F(\tilde{L})$ according to

$$k\frac{\partial}{\partial k}U_k(\rho) = \frac{k^5}{4\pi Z_k}G_1(T)F(\tilde{L}) + \eta\rho U_k'(\rho). \tag{16}$$

The universal part reads

$$G_1(T) = \left(\sqrt{\frac{1+w_1}{1+w_2}} + \sqrt{\frac{1+w_2}{1+w_1}}\right)$$
$$\times \left[\frac{1}{2} + N_B\left(\frac{k^2\sqrt{(1+w_1)(1+w_2)}}{Z_k}\right)\right], \tag{17}$$

with $w_1 = U'/k^2$, $w_2 = (U' + 2\rho U'')/k^2$, and the Bose function $N_B(x) = (e^{x/T} - 1)^{-1}$. Here a prime denotes a derivative with respect to ρ. Further, η constitutes the k-dependent anomalous dimension associated with field rescaling. For a detailed derivation of Eq. (16) see Appendix B.

The influence of the trap is encoded in the crossover function $F(\tilde{L})$, which for pbc is given by

$$F_{\mathrm{pbc}}(\tilde{L}) = \frac{2N+1}{\tilde{L}}\left[1 - \frac{\eta}{4} - \frac{1}{\tilde{L}^2}\left(1 - \frac{\eta}{2}\right)\frac{4\pi^2}{3}N(N+1)\right.$$
$$\left. - \frac{\eta}{\tilde{L}^4}\frac{4\pi^4}{15}N(N+1)(-1+3N+3N^2)\right], \tag{18}$$

with $\tilde{L} = Lk$, $N = \lfloor\frac{\tilde{L}}{2\pi}\rfloor$, and $\lfloor x \rfloor$ being the largest integer $< x$. The function F interpolates between the 3D and the 2D flow equations via the two limiting cases

$$F(\tilde{L}) = \begin{cases} \frac{2}{3\pi}\left(1 - \frac{\eta}{5}\right) & (\tilde{L} \gg 1), \\ \tilde{L}^{-1}\left(1 - \frac{\eta}{4}\right) & (\tilde{L} \ll 1). \end{cases} \tag{19}$$

We plot the crossover function for pbc in Fig. 2. One observes a rather sharp transition from 3D behavior for $k > \frac{2\pi}{L}$ to 2D behavior for $k < \frac{2\pi}{L}$. The oscillatory behavior in the transition region is rapidly damped. The flow equation for the dashed lines corresponds precisely to the flow in three or two dimensions with the same truncation. Dimensional reduction is very effectively realized by the flow with a reasonable approximation simply switching from three to two dimensions
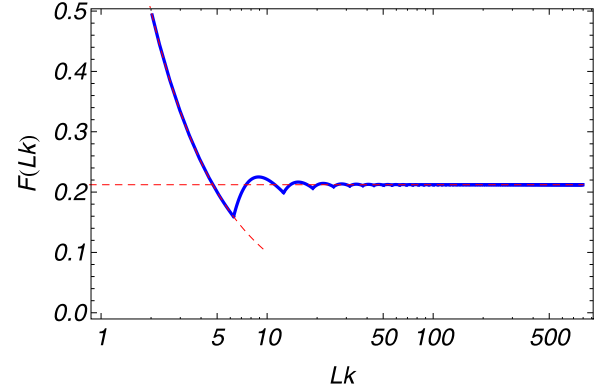

FIG. 2. The crossover function $F(\tilde{L})$ modifies the flow equations of the 3D system. For small $\tilde{L} = Lk$ it diverges like $\tilde{L}^{-1}$ and the 2D flow equations are recovered. For large $\tilde{L}$ it approaches a constant and the system behaves three-dimensionally. In the FRG approach we start at an ultraviolet scale $k_\Lambda = \Lambda$ with $L\Lambda \gg 1$, so that the description of the microscopic theory is three-dimensional.

as k decreases below $2\pi/L$. A similar sharp transition has been observed in the τ direction for the transition between quantum and classical statistics [51,52].

From Eq. (16), the flow equations of $U_k'(\rho_0)$ and $\lambda_k = U_k''(\rho_0)$ follow by simple differentiation with respect to ρ. The flow of the location of the minimum $\rho_{0,k}$ is obtained by

$$\frac{\partial}{\partial k}\rho_{0,k} = -\lambda_k^{-1}\frac{\partial}{\partial k}U_k'\bigg|_{\rho_0}. \tag{20}$$

By following the flow of $\rho_{0,k}$ for $k \to 0$ we deduce whether $\rho_{0,0} > 0$ (superfluid phase) or $\rho_{0,0} = 0$ (disordered phase). This allows us to extract the superfluid transition temperature T_{c} for all trap sizes L. We determine the density by a suitable flow equation (see Ref. [24]).

We plot the superfluid fraction ρ_0/n for different values of L in Fig. 3. Note that even for a 2D system the ratio ρ_0/n of the 3D quantities ρ_0 and n gives the superfluid fraction, since
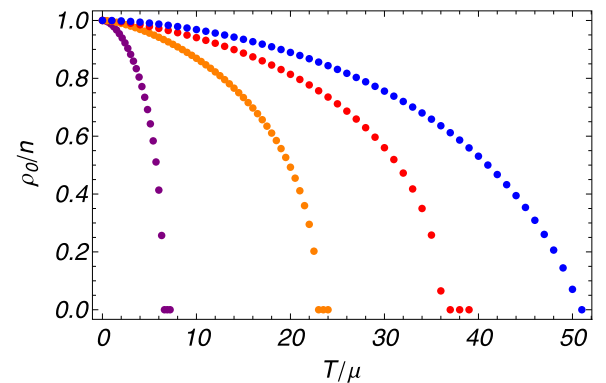

FIG. 3. Superfluid fraction ρ_0/n at $k \to 0$ for different values of L. Larger values of L correspond to the curves farther to the right. We directly see that the critical temperature, here in units of the chemical potential μ, is higher in more 3D-like systems. For all compactification lengths L we recover the correct limit $\rho_0/n|_{T\to 0} = 1$, where the whole gas is superfluid due to Galilean invariance. Curves correspond to a coupling strength $g_{3D}\sqrt{\mu} = 0.025$.
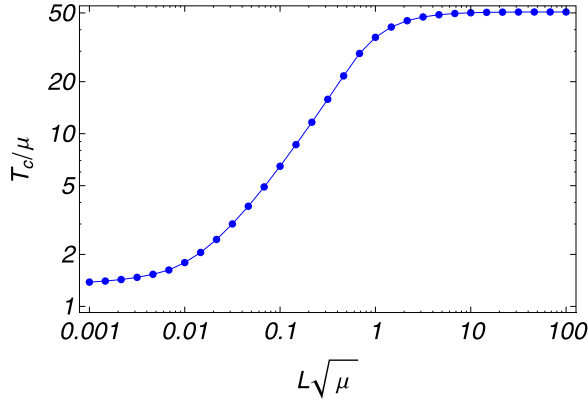
FIG. 4. Dimensional crossover of the superfluid critical temperature T_c from two to three dimensions. For large L the superfluid transition goes along with Bose-Einstein condensation. The transition temperature is substantially lower in a smaller system, i.e., when L is smaller. For the crossover we fix the 3D coupling constant to the same value as in Fig. 3. In experiments with ultracold atoms, g_{3D} is usually controlled by a magnetic Feshbach resonance.

$\rho_0^{2D} = L\rho_0^{3D}|_{L\to 0}$ and $n^{2D} = Ln^{3D}|_{L\to 0}$, so that L drops out. For vanishing temperature the whole gas becomes superfluid irrespective of L and develops a small condensate depletion due to interactions [24].

In Fig. 4 we show the superfluid transition temperature T_c for the whole 2D-3D dimensional crossover. For large L, T_c approaches the Bose-Einstein condensation (BEC) temperature T_{BEC} of the interacting gas, given by

$$T_{BEC} = T_{c,id} + \Delta T_c,$$

$$T_{c,id} = \frac{2\pi\hbar^2}{Mk_B}\left(\frac{n}{\zeta(3/2)}\right)^{2/3} = 6.625 n^{2/3}. \quad (21)$$

The interaction-induced shift of the critical temperature [53,54] for a sufficiently small gas parameter $a_{3D}n^{1/3}$ reads

$$\frac{\Delta T_c}{T_{c,id}} = \kappa\, a_{3D}n^{1/3}. \quad (22)$$

Within our calculation we have $\kappa = 2.1$ [24], which compares well with the Monte Carlo result [55–57]. In our setup we define g_{3D} by

$$g_{3D} = 8\pi a_{3D} = \lambda_{3D,k\to 0}. \quad (23)$$

In terms of the chemical potential we find $T_c/\mu = 51$ for $g_{3D}\sqrt{\mu} = 0.025$, which corresponds to $\mu_c = 1.9 g_{3D}n$ at the transition. Note that Hartree-Fock theory predicts $\mu = 2g_{3D}n$ above the transition temperature.

As L is lowered towards the 2D case, the critical temperature decreases and is reduced by a substantial factor as one goes through the crossover. Here we perform the dimensional crossover for a fixed value of $a_{3D} = g_{3D}/(8\pi)$, since this quantity is typically fixed by the magnetic field in cold-atom experiments. This, in turn, fixes the initial 3D coupling λ_Λ^{3D} through Eq. (36) and leads to a characteristic behavior of T_c in the 2D limit of small L. For this note that for $L \gtrsim \Lambda^{-1}$ the flow in Eq. (16) is solely determined by $F(\tilde{L}) \simeq \tilde{L}^{-1}(1 - \frac{\eta}{4})$ and, thus, resembles a truly 2D renormalization group flow. In particular, this applies to the initial value of the coupling,

which for $L \to 0$ is given by

$$\lambda_{2D,\Lambda}\bigg|_{L\Lambda \gtrsim 1} = \frac{1}{L}\lambda_{3D,\Lambda} \approx 8\pi\frac{a_{3D}}{L} \quad (24)$$

[see Eq. (43)]. Hence, as we decrease L in this regime, we simulate a whole class of strongly interacting 2D Bose gases, each corresponding to a certain coupling $\lambda_{2D}(L)$ and critical temperature $T_c(L)$. Consequently, T_c does not fully saturate for small L, as can be seen in Fig. 4, although the dependence becomes weak.

In cold-atom experiments, the 2D coupling strength is commonly expressed by the coupling constant $\tilde{g} = (M/\hbar^2)g_{2D} = g_{2D}/2$. Due to the logarithmic energy dependence of the T matrix in two dimensions, the coupling g_{2D} needs to be defined with respect to a fixed energy or momentum scale (in contrast to a_{2D}). On the other hand, as this scale dependence is only logarithmic, $\tilde{g}$ appears to be effectively constant in experiments. One convenient choice consists in defining the coupling at the momentum scale $k_n = \sqrt{n_{2D}}$ related to the 2D density $n_{2D} = Ln_{3D}$. For studying the phase transition, $T > \mu$ sets the appropriate scale and thus for a true 2D system we define

$$g_{2D} = 2\tilde{g} = \lambda_{2D,k=\sqrt{T}} \quad (25)$$

in the FRG approach. Another convenient choice consists in identifying the expression in Eq. (24) with g_{2D}.

For a true 2D system with small $\tilde{g}$, the critical phase-space density for the BKT transition is $n\lambda_T^2 = \ln(\xi/\tilde{g})$, where $\lambda_T^2 = \frac{2\pi\hbar^2}{Mk_BT} = \frac{4\pi}{T}$. Monte Carlo calculations yield $\xi = 380$ [31,32]. Hence the 2D critical temperature reads

$$T_{BKT} = \frac{4\pi n_{2D}}{\ln(\xi/\tilde{g})}. \quad (26)$$

By employing $\mu_c/T = (\tilde{g}/\pi)\ln(\xi_\mu/\tilde{g})$ for the critical chemical potential, we may also express the critical temperature for small $\tilde{g}$ as

$$\frac{T_{BKT}}{\mu} = \frac{\pi}{\tilde{g}}\frac{A}{\ln(\xi_\mu/\tilde{g})}. \quad (27)$$

Here $A = 1$ and $\xi_\mu = 13.2$ from Monte Carlo computations [31]. In our setup, the values of A and ξ_μ mildly depend on the value of k_f introduced at the beginning of this section (see the discussion in Ref. [25] and Appendix A1. For the choice of k_f applied here we find $A \simeq 1$ and $\xi_\mu \simeq 6$. The parametric form in Eq. (27) has also been obtained with the FRG in Ref. [29], where T_{BKT} was determined in a manner different from that employed here, yielding $A = 0.982$ and $\xi_\mu = 9.48$.

For experiments with ultracold 2D gases it might be relevant that a finite extension in the z direction leads to an enhanced superfluid transition temperature. Depending on the system this influence can be quite substantial. For a related study in the context of BCS superfluidity of two-component fermions, see Ref. [58], where an enhancement of the critical temperature in a quasi-2D geometry has been found. Furthermore, since in three dimensions we also have a macroscopic occupation of the lowest-energy state, which is a condensate, there might still be some residual condensate for small yet finite L and nonvanishing temperatures.

To investigate the question whether the partial influence of the third dimension influences the critical temperature of a (supposed to be) 2D system, we perform the dimensional crossover for a fixed value of a_{2D}. Note that this is in contrast to the data shown in Figs. 3 and 4, where a_{3D} is kept fixed. In Appendix A1, we provide a discussion of the dimensional crossover of T_c/μ for small L and fixed a_{2D}. We find that for sufficiently small L/a_{2D}, the critical temperature coincides with that of the true 2D system and is then *enhanced* for larger values of L.

IV. TWO-DIMENSIONAL LIMIT

A. Effective 2D coupling constant

We have seen that the flow of couplings can be described by a 2D flow whenever the scale k is below an effective cutoff $\Lambda_{\rm eff} \ll L^{-1}$. In particular, if L^{-1} is much larger than the many-body scales $\sqrt{\mu}$ and $\sqrt{T}$, the many-body system can be described by an effective 2D model with UV cutoff $\Lambda_{\rm eff}$. We call this scenario the 2D limit. The aim of this section is to relate the $\lambda_{2D}(\Lambda_{\rm eff})$ value of the effective 2D action to the 3D scattering length. By integrating the flow equations between Λ and $\Lambda_{\rm eff}$ in vacuum, we obtain the relation between a_{2D} and a_{3D}, which depends on the particular compactification or trap potential. Once the renormalized coupling $\lambda_{2D}(\Lambda_{\rm eff})$ is specified, it allows us to universally determine the many-body properties of the effective 2D system, and no further knowledge of the 3D system is required.

In terms of the flow equation, (16), the 2D limit manifests itself in the fact that the prefactor $F(\tilde{L})$ approaches the regime $\tilde{L} = Lk \ll 1$ much earlier than any of the many-body scales is resolved. We introduce the momentum scale $\Lambda_{\rm eff}$ via

$$\Lambda \gg L^{-1} \gg \Lambda_{\rm eff} \gg \sqrt{\mu}, \sqrt{T}. \tag{28}$$

The scale $\Lambda_{\rm eff}$ is arbitrary within these constraints and serves as a UV cutoff of the effective 2D theory.

In the following we consider the regime $k \in [\Lambda_{\rm eff}, \Lambda]$ of the RG flow. It is characterized by $Z_k = 1$, $\eta = \rho_{0,k} = N_B = 0$, leading to a simple form of Eq. (16), which reads

$$\dot{U}(\rho) = \frac{k^5}{8\pi} F_0(\tilde{L}) \left(\sqrt{\frac{1 + w_1}{1 + w_2}} + \sqrt{\frac{1 + w_2}{1 + w_1}} \right), \tag{29}$$

where the over dot denotes a derivative with respect to $t = \ln(k/\Lambda)$. The crossover function $F|_{\eta=0} = F_0$ is evaluated for $\eta = 0$ [see Eq. (B34) for pbc]. In particular, for $\tilde{L} \ll 1$ we are left with

$$\dot{U}(\rho) = \frac{1}{L} \frac{k^4}{8\pi} \left(\sqrt{\frac{1 + w_1}{1 + w_2}} + \sqrt{\frac{1 + w_2}{1 + w_1}} \right) = \frac{1}{L} \dot{U}_{2D}. \tag{30}$$

This is, up to the prefactor L^{-1}, the flow equation of the 2D potential defined via $U_{3D} = \frac{1}{L} U_{2D}$ and $\rho_{3D} = \frac{1}{L} \rho_{2D}$. Note that by this definition the quantities $w_1 = U'_{3D}/k^2 = U'_{2D}/k^2$ and $w_2 = (U'_{3D} + 2\rho_{3D}U''_{3D})/k^2 = (U'_{2D} + 2\rho_{2D}U''_{2D})/k^2$ are invariant. We define $\lambda^{2D} = U''_{2D}(0)$ in a vacuum such that the effective 2D coupling strength at scale $\Lambda_{\rm eff}$ is given by

$$\lambda^{2D}_{\Lambda_{\rm eff}} = \frac{1}{L} \lambda^{3D}_{\Lambda_{\rm eff}}. \tag{31}$$

The running of the 3D coupling constant $\lambda_k = \lambda^{3D}_k = U''_{3D}(0)$ in vacuum is found to be

$$\dot{\lambda}_k = \frac{k^5}{4\pi} F_0(\tilde{L}) \frac{\lambda^2_k}{k^4}. \tag{32}$$

In order to solve this equation we write

$$\partial_k \frac{1}{\lambda_k} = -\frac{1}{4\pi} F_0(\tilde{L}) \tag{33}$$

and arrive at

$$\frac{1}{\lambda^{3D}_{\Lambda_{\rm eff}}} - \frac{1}{\lambda^{3D}_\Lambda} = \frac{1}{4\pi L} \int_{L\Lambda_{\rm eff}}^{L\Lambda} d\tilde{L} \, F_0(\tilde{L}). \tag{34}$$

Using Eq. (31) we obtain

$$\frac{1}{\lambda^{2D}_{\Lambda_{\rm eff}}} = \frac{L}{\lambda^{3D}_\Lambda} + \frac{1}{4\pi} \int_{L\Lambda_{\rm eff}}^{L\Lambda} d\tilde{L} \, F_0(\tilde{L}). \tag{35}$$

The coupling constants λ^{3D}_Λ and $\lambda^{2D}_{\Lambda_{\rm eff}}$ can be related to the 3D and 2D scattering lengths a_{3D} and a_{2D} by means of the formulas

$$\frac{1}{\lambda^{3D}_\Lambda} = -\frac{\Lambda}{6\pi^2} + \frac{1}{8\pi a_{3D}}, \tag{36}$$

$$\frac{1}{\lambda^{2D}_{\Lambda_{\rm eff}}} = -\frac{1}{8\pi} \ln \left(\Lambda^2_{\rm eff} a^2_{2D} \right) + \frac{1}{8\pi} \tag{37}$$

[see Eqs. (C15) and (C16)]. Inserting these relations into Eq. (35) we find

$$a_{2D} = L \exp \left\{ -\frac{1}{2} \frac{L}{a_{3D}} + \Phi \right\}, \tag{38}$$

with

$$\Phi = \frac{2L\Lambda}{3\pi} - \ln(L\Lambda_{\rm eff}) + \frac{1}{2} - \int_{L\Lambda_{\rm eff}}^{L\Lambda} d\tilde{L} \, F_0(\tilde{L}). \tag{39}$$

Note that the artificial scales $\Lambda_{\rm eff}$ and Λ drop out due to the particular limits of $F(\tilde{L})$ in Eq. (19) and we can deduce a_{2D} purely from the values of a_{3D} and L. This is true for any crossover function $F(\tilde{L})$ that satisfies (19) and approaches these limits sufficiently rapidly in the variable $\tilde{L}$.

For a confinement along the z direction with pbc we numerically find $\Phi = 0$ and are thus left with

$$a^{(\rm pbc)}_{2D} = L \exp \left\{ -\frac{1}{2} \frac{L}{a_{3D}} \right\}. \tag{40}$$

Since Λ drops out of the formula, the new effective cutoff of the 2D theory is given by L^{-1}. In particular, this formula should be compared with the result in a harmonic trap [1,59,60] given by

$$a_{2D} = \ell_z \sqrt{\frac{\pi}{A}} \exp \left\{ -\sqrt{\frac{\pi}{2}} \frac{\ell_z}{a_{3D}} \right\}, \tag{41}$$

with $A = 0.905$ and $\ell_z = \sqrt{\hbar/M\omega_0}$ the oscillator length. We may identify the effective length scale $\ell^{\rm eff}_z = L/\sqrt{2\pi}$ and an effective constant $A_{\rm eff}$ to match our results to Eq. (41) according to

$$a_{2D} = \ell^{\rm eff}_z \sqrt{\frac{\pi}{A_{\rm eff}}} \exp \left\{ -\sqrt{\frac{\pi}{2}} \frac{\ell^{\rm eff}_z}{a_{3D}} \right\}. \tag{42}$$

We have $A^{(\rm pbc)}_{\rm eff} = \frac{1}{2}$ for the case of pbc.

Note also that Eqs. (31) and (36) imply

$$\lambda_{2\mathrm{D},\Lambda_{\mathrm{eff}}} = \frac{1}{L}\lambda_{3\mathrm{D},\Lambda_{\mathrm{eff}}} = \frac{1}{\frac{L}{8\pi a_{3\mathrm{D}}} - \frac{L\Lambda_{\mathrm{eff}}}{6\pi^2}}. \quad (43)$$

If $a_{3\mathrm{D}}/L \to 0$ is sufficiently small, we can ignore the term of order $O(L\Lambda_{\mathrm{eff}})$ in the denominator. Furthermore, neglecting the logarithmic running of the coupling, we can identify $g_{2\mathrm{D}} \approx \lambda_{2\mathrm{D},\Lambda_{\mathrm{eff}}}$ and thus arrive at

$$g_{2\mathrm{D}} \approx 8\pi \frac{a_{3\mathrm{D}}}{L}. \quad (44)$$

Written in terms of $\tilde{g} = g_{2\mathrm{D}}/2$ and ℓ_z^{eff} this assumes the familiar form

$$\tilde{g} \approx \sqrt{8\pi}\frac{a_{3\mathrm{D}}}{\ell_z^{\mathrm{eff}}}, \quad (45)$$

known from the case of harmonic confinement [1].

B. *T* matrix

The scattering properties of bosons in the dimensional crossover are naturally included in the FRG flow equations in the limit of vanishing density and temperature. Here we compare and benchmark our findings with the quantum mechanical T-matrix approach to low-energy scattering, where the particle-particle loop is integrated directly without the use of a flow equation. In Appendix C we give a detailed discussion of the interrelation of both approaches and limit this presentation to the main results. The fact that the flow equation for the T matrix in vacuum can be solved exactly is related to a decoupling property of the two-body sector in this particular system; see Ref. [61] for an extensive analysis. The route to determining the scattering properties of two particles in a box potential via the T matrix has also been explored in Ref. [62], and Eqs. (40) and (55) here agree with the results therein for $L = 2\pi R$.

To compute the T matrix we utilize a sharp momentum cutoff which equips the momentum integration with a UV cutoff scale Λ. This regularization differs from the use of the regulator $R_k(Q)$ in Eq. (B8). We make this explicit by adding the superscript (sh) to the microscopic coupling, $\lambda_\Lambda^{(\mathrm{sh})}$. One result of the analysis in Appendix C is to relate $\lambda_\Lambda^{(\mathrm{sh})}$ to λ_Λ, the latter being used in the FRG analysis in Eqs. (36) and (37). Note at this point that it is difficult to obtain the additional term $+\frac{1}{8\pi}$ in Eq. (37) without computing the energy dependence of the T matrix.

The low-energy T matrix $T(E)$ in D noncompact dimensions is defined as

$$\frac{1}{T(E)} = \frac{1}{\lambda_\Lambda^{(\mathrm{sh})}} - \int_{\tilde{q}}^{\Lambda} \frac{1}{E + i0 - 2q^2}, \quad (46)$$

where $2q^2 = q^2/2M_r$ with reduced mass $M_r = M/2$ (see, for instance, Refs. [60] and [63] for a detailed discussion). In three dimensions the integration yields

$$\frac{1}{T^{3\mathrm{D}}(E)} = \frac{1}{8\pi}\left(\frac{1}{a_{3\mathrm{D}}} - \sqrt{-(E + i0)/2}\right) \quad (47)$$

provided we choose

$$\frac{1}{\lambda_{3\mathrm{D},\Lambda}^{(\mathrm{sh})}} = -\frac{\Lambda}{4\pi^2} + \frac{1}{8\pi a_{3\mathrm{D}}}. \quad (48)$$

In the 2D case we have

$$\frac{1}{T^{2\mathrm{D}}(E)} = -\frac{1}{8\pi}\ln\left(-\frac{(E + i0)a_{2\mathrm{D}}^2}{2}\right)$$

$$= -\frac{1}{8\pi}\left[\ln\left(\frac{Ea_{2\mathrm{D}}^2}{2}\right) - i\pi\right] \quad (49)$$

and

$$\frac{1}{\lambda_{2\mathrm{D},\Lambda}^{(\mathrm{sh})}} = -\frac{1}{8\pi}\ln\left(\Lambda^2 a_{2\mathrm{D}}^2\right). \quad (50)$$

These universal forms of the T matrix for low-energy scattering in three and two dimensions serve as definitions of the scattering lengths $a_{3\mathrm{D}}$ and $a_{2\mathrm{D}}$.

We now consider the generalization of $T(E)$ when the z direction is confined in a well of size L with pbc. We then have the quantization $q_z \to k_n$, $n \in \mathbb{Z}$, for momenta in the z direction, and

$$\int_{-\infty}^{\infty} \frac{dq_z}{2\pi} \to \sum_{n=-\infty}^{\infty} \frac{\Delta k_n}{2\pi} = \frac{1}{L}\sum_{n=-\infty}^{\infty}. \quad (51)$$

The zero-point energy vanishes for this particular choice of confinement. We write $A = -(E + i0)/2$ and find

$$\frac{1}{T(E,L)} = \frac{1}{\lambda_{3\mathrm{D},\Lambda}^{(\mathrm{sh})}} + \frac{1}{2L}\sum_n \int^{\Lambda'} \frac{d^2q}{(2\pi)^2}\frac{1}{k_n^2 + q^2 + A}$$

$$= \frac{1}{\lambda_{3\mathrm{D},\Lambda}^{(\mathrm{sh})}} + \frac{1}{2}\int^{\Lambda'} \frac{d^2q}{(2\pi)^2}\frac{\frac{1}{2} + n_B(L\sqrt{q^2 + A})}{\sqrt{q^2 + A}}$$

$$= \frac{1}{\lambda_{3\mathrm{D},\Lambda}^{(\mathrm{sh})}} + \frac{\Lambda' - \sqrt{A}}{8\pi} - \frac{1}{4\pi L}\ln(1 - e^{-L\sqrt{A}}), \quad (52)$$

with $n_B(x) = (e^x - 1)^{-1}$. For $L = \infty$, the result is finite in the limit $E \to 0$. It reduces to the 3D expression, (47), provided we choose

$$\frac{1}{\lambda_{3\mathrm{D},\Lambda}^{(\mathrm{sh})}} = -\frac{\Lambda'}{8\pi} + \frac{1}{8\pi a_{3\mathrm{D}}}, \quad \Lambda' = \frac{2}{\pi}\Lambda. \quad (53)$$

(Note that Λ and Λ' are UV cutoffs for 3D and 2D continuous momenta, respectively, and thus do not need to coincide.) More formally we define

$$\frac{1}{8\pi a_{3\mathrm{D}}} := \lim_{E \to 0}\lim_{L \to \infty}\frac{1}{T(E,L)}. \quad (54)$$

We thus have

$$\frac{1}{T(E,L)} = \frac{1}{8\pi}\left(\frac{1}{a_3} - \sqrt{A}\right) - \frac{1}{4\pi L}\ln(1 - e^{-L\sqrt{A}}). \quad (55)$$

For $L < \infty$, the T matrix develops a logarithmic IR singularity as $E \to 0$. In particular, we find for the effective 2D

T matrix

$$\frac{1}{T_{\mathrm{2D}}(E)} := \frac{L}{T(E,L)} \overset{A\to 0}{\simeq} \frac{L}{8\pi a_{\mathrm{3D}}} - \frac{1}{4\pi}\ln(L\sqrt{A})$$

$$= \frac{L}{8\pi a_{\mathrm{3D}}} - \frac{1}{4\pi}\ln\left(L\sqrt{-\frac{(E+i0)}{2}}\right)$$

$$\overset{!}{=} -\frac{1}{4\pi}\ln\left(a_{\mathrm{2D}}\sqrt{-\frac{(E+i0)}{2}}\right)$$

$$= -\frac{1}{8\pi}\ln\left(-\frac{(E+i0)a_{\mathrm{2D}}^2}{2}\right). \tag{56}$$

We observe the effective 2D scattering length of the confined system to be

$$a_{\mathrm{2D}}^{(\mathrm{pbc})}(L) = L\exp\left\{-\frac{1}{2}\frac{L}{a_{\mathrm{3D}}}\right\}. \tag{57}$$

This result agrees with the FRG finding in Eq. (40).

V. DISCUSSION

In this work we have studied the dimensional crossover of nonrelativistic bosons when confining a transverse spatial dimension. Although the derived set of flow equations is applicable to crossovers from $(D+1)$ to D dimensions, our main focus has been on the crossover from three to two dimensions. The motivation for this is the intriguing nature of the superfluid transition in this case and the considerable number of recent cold-atom experiments on this topic. Especially, we wish to contribute to a few open theoretical challenges in the interpretation of the data of these as outlined below.

The present approach may, however, be extended to describe further dimensional crossovers in condensed matter systems. Compactifications from two dimensions to one, or from three dimensions to one, are highly exciting from the point of view of quantum phase transitions. Indeed, phases with quasi-long-range order may survive in one dimension at zero temperature and are conceptually close to the finite-temperature superfluid phase in a 2D Bose gas; see, for instance, Ref. [23] for an FRG perspective on this aspect and Ref. [45] for a mean-field study of the correlations in the dimensional crossover from three to two dimensions (one dimension) at $T > 0$ ($T = 0$). Since the confinement only affects spatial momenta, the characteristic frequency dependence which governs quantum critical phenomena will be resolved correctly with the FRG in the dimensional crossover if this is the case for the system without compact dimensions. The nature of inhomogeneous phases of fermion pairs in dimensional crossovers has been discussed in Refs. [64] and [65].

As an effective description of bosonic degrees of freedom, the finite-temperature 2D Bose gas and its BKT transition may also be applied to the pseudogap phase of underdoped cuprates [66]. The inherent nonrelativistic nature of complex bosonic degrees of freedom is also found in open or nonequilibrium quantum systems such as exciton-polariton condensates in semiconductor microcavities [67,68]. The Keldysh field theory techniques required to describe such systems can be incorporated into the FRG framework (see Ref. [69] for an introduction).

In our analysis of the superfluid phase transition we have performed the dimensional crossover in two variants: for fixed a_{3D} and for fixed a_{2D}. Each procedure addresses a somewhat different question. When fixing a_{3D} we follow the typical cold-atom experimental protocol of setting the value of a_{3D} by means of an external magnetic field B and then decreasing the length L to eventually arrive at a 2D system. Importantly, the size of L is typically not easily tunable in experiments but, rather, fixed to a particular value. We can then reach a large class of values for a_{2D} by means of formula (40) by changing $a_{\mathrm{3D}}(B)$. In view of Fig. 4, where $g_{\mathrm{3D}}\sqrt{\mu} = 0.025$, one experiment corresponds to one certain point $L\sqrt{\mu}$ on the abscissa. Through Eq. (24) this corresponds to a certain value of g_{2D}. If one were to perform the experiment with a different value of L, one would simulate a different Bose gas (with different g_{2D}) for the same value of a_{3D}. In order to plan and devise an experimental setup it is crucial to know the effective a_{2D} and g_{2D} which can be reached for a given L, and formulas (41) and (45) are abundantly applied in the experimental cold-atom literature.

On the other hand, in view of attempting to quantum simulate 2D systems, we may ask: Given $L \neq 0$, can we be sure that we are measuring the critical temperature of the 2D system and not that of its quasi-2D relatives? By fixing a_{2D} (instead of a_{3D}) for small L in the dimensional crossover we confirm with the study in Appendix A2, that the critical temperature is enhanced by the residual influence of the third dimension. This is not too surprising, as we expect the possibility of Bose condensation in $D > 2$ to greatly increase the critical temperature. Furthermore, we found that the true 2D critical temperature is realized for a considerable range of (L/a_{2D}) values.

Our discussion of the low-energy T matrix to describe the scattering properties of the Bose gas was mostly inspired by the aim to benchmark relation (40) between the 3D and the 2D scattering lengths obtained with the FRG. However, given an exact or approximate expression for the T matrix of the confined system, the obstacle of analyzing current cold-atom experiments can be resolved: At high densities—especially for fermionic systems, which do not differ from the bosonic counterparts in their scattering properties—the typical momenta of particles are not necessarily low. Hence one needs to restrict the experiment to low densities, or the scattering cross sections and effective coupling constants need to be evaluated at a finite momentum [70–73]. This may effectively be accomplished with the energy- and momentum-resolved T matrix of the confined system, with its particular discrete mode spectrum such as in Eq. (55). To resolve this mode spectrum, one may actually restrict oneself to phenomenological collective mode spectra such as in Refs. [74–76]. Complementary approaches to obtaining the scattering properties inside a medium from the vacuum T matrix, however, for a true 2D system, have been successfully applied, for instance, to the Fermi polaron problem [77].

Upon confining the gas by means of a potential well with pbc, the challenging task of determining the interacting ground state of the system became particularly simple: The ground state is still homogeneous in space and given by the minimum of the effective potential $U_{k\to 0}(\phi^2)$. However, as discussed at the end of Sec. II, the situation becomes more complicated

already for a box potential with infinite walls. Whereas in a Hamiltonian formulation the ground states of the interacting system are required to compute the expectation values of observables, the interacting ground state enters the functional integral formulation by the need to evaluate the effective action $\Gamma[\phi]$ at its minimum configuration $\phi_0(\tau, \vec{x})$. The latter, however, will not be constant in space for a trapped system, i.e., we are dealing with an inhomogeneous ground state. Thus, strictly speaking, the ground state can no longer be found by minimizing the effective potential $U_{k\to 0}(\phi^2)$ evaluated for constant fields. Still one might define a suitable modification of the effective potential which captures the energy of the lowest-lying excitations, which might be modeled in a first approximation by the noninteracting states or deformations thereof.

Finally, we discuss the relevance of our findings for trapping potentials different from a well with pbc. The main difference in trapping the system in a box potential versus a harmonic trap consistsin the facts (i) that the ground states of the latter are inhomogeneous and (ii) that the related ground-state energies E_0 are nonzero. We have addressed the first point in the previous paragraph. In fact, it should constitute the main technical difficulty in the computation of different confinement scenarios with the FRG.

To understand the role of point (ii), note that the emergent 2D scattering physics relied on a logarithmic singularity of the effective 2D T matrix as $E \to 0$ [see Eq. (56)]. This divergence allows us to read off the effective 2D scattering length. For a system with nonvanishing E_0, the logarithmic divergence will appear for $\Delta E \to 0$, where $E = E_0 + \Delta E$. This is true for harmonic confinement [59,60], and a preliminary calculation for the T matrix in a box suggests that the same pattern appears, with a formula relating a_{3D} and a_{2D} analogous to Eq. (40). Consequently, the emergent 2D physics appear in the effective 2D continuum of states just above the zero-point energy (see Fig. 1). Subtracting the shift of energies due to E_0, e.g., by a chemical potential or by evaluating the "effective potential" at a nonzero frequency, the remaining field theory describing scattering and the superfluid phase transition will be very similar to the one considered here with pbc. In fact, we have shown that Eqs. (40) and (44) are in one-to-one correspondence with the results for harmonic confinement with ℓ_z once we identify $\ell_z^{\text{eff}} = L/\sqrt{2\pi}$ as the effective oscillator length of the potential well.

ACKNOWLEDGMENTS

APPENDIX A: SUPERFLUID TRANSITION IN THE 2D LIMIT

1. Critical temperature in two dimensions

The limiting formula, (27), for the critical temperature of a 2D superfluid Bose gas can be studied independently of the
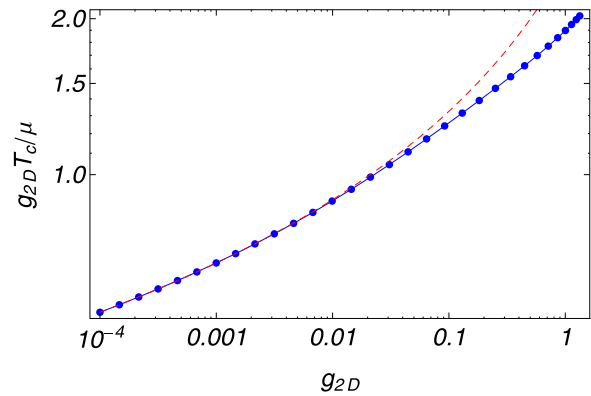

FIG. 5. Critical temperature T_c/μ in two dimensions as a function of g_{2D} over four orders of magnitude. For better comparability with Eq. (A2) we have multiplied the function by g_{2D}. The blue circles and solid line constitute the FRG result for $t_f = -10$ (as used in the text), whereas the dashed red line corresponds to the asymptotic form of Eq. (A2) for small g_{2D}. For the dashed line we use the fit result from Table I.

details of the dimensional crossover. For this purpose we set $\Lambda/\sqrt{\mu} = 10^3$ as in the text and vary the values of $t_f = \ln(k_f/\Lambda)$ and $\lambda_{2D,\Lambda}$. We define

$$g_{2D} = \lambda_{2D,k=\sqrt{T}} \tag{A1}$$

as in Eq. (25).

For $t_f = -10$, as employed in the text, we find the g_{2D} dependence of T_c/μ to be in good agreement with the asymptotic form of Eq. (27), i.e.,

$$\frac{T_c}{\mu} = \frac{2\pi}{g_{2D}} \frac{A}{\ln(2\xi_\mu/g_{2D})}, \tag{A2}$$

when choosing $A = 0.99$ and $\xi_\mu = 6.0$. We illustrate the coupling dependence of the critical temperature in Fig. 5. Upon varying t_f in a reasonable range, we consistently find scaling according to Eq. (A2) with only mild variations of the parameters A and ξ_μ, which we list in Table I. The corresponding values have been obtained from a fit of T_c/μ to Eq. (A2) in the interval $g_{2D} \in [10^{-4}, 0.01]$.

2. Dimensional crossover for fixed a_{2D}

In order to perform the dimensional crossover for fixed a_{2D} we need to choose the initial conditions of the flow rather carefully. Here we collect the technical details and parameters which allow us to conclude that the critical temperature of the 2D gas is enhanced by the influence of a sufficiently large third dimension.

TABLE I. Fitting parameters obtained by matching the critical temperature T_c/μ for different values of $t_f = \ln(k_f/\Lambda)$ to Eq. (A2) in the interval $g_{2D} \in [10^{-4}, 0.01]$.

	t_f				
	-8	-9	-10	-11	-12
A	0.94	0.98	0.99	0.99	0.99
ξ_μ	5.1	5.3	6.0	6.6	7.2

First, note that Eq. (36) implies that a_{3D} cannot be arbitrarily large within our model with pointlike interactions. Indeed, for fixed Λ, the scattering length is bounded from above according to $a_{3D} < a_{max} = (\frac{4\Lambda}{3\pi})^{-1} = 2.36\Lambda^{-1}$ [24]. In particular, for $\Lambda \to \infty$ we have $a_{3D} \to 0$, meaning that the pointlike approximation cannot describe the interacting system up to arbitrarily high energies. For fixed L this implies $a_{2D} < Le^{-\frac{1}{2}(L/a_{max})}$ due to Eq. (40). Thus, in typical experiments with fixed L, the range of accessible a_{2D} is also limited from above.

On the other hand, one may fix a_{2D} and Λ and determine the possible values of L which realize this particular a_{2D}. This leads us to considering the function $f(x) = 4\pi a_{2D}/\lambda_\Lambda^{3D} = \frac{\ln(x)}{x} - \frac{2}{3\pi}(\Lambda a_{2D})$ with $x = L/a_{2D}$. A stable solution requires $f(x)$ to be positive, leading to a stability interval $[L_{min}, L_{max}]$ of possible L values. From Eqs. (50) and (C16) we see that, disregarding some modifications due to the regularization procedure, we have $\Lambda a_{2D} < 1$. For instance, choosing $\Lambda a_{2D} = 0.1$ (0.01) we arrive at $x_{min} \simeq 1.02$ (1.002) and $x_{max} \simeq 260$ (3900). The corresponding value of L_{min}, however, will typically be too small, as we also need to satisfy $L\Lambda \gg 1$.

For our discussion of the dimensional crossover at fixed a_{2D} we employ $\mu = 1$, $a_{2D} = 10^{-3}$, $\Lambda = 10$, $k_f = 10^{-2}$ and vary L within the boundaries allowed by these constraints. We choose $L_{min} = \Lambda^{-1}$ from $L\Lambda > 1$ and $L_{max} = 3885a_{3D}$ from the positivity of $f(x)$. The critical temperature of the pure 2D gas for this choice of parameters is $T_c/\mu = 1.32$. The resulting crossover of the critical temperature is shown in Fig. 6.
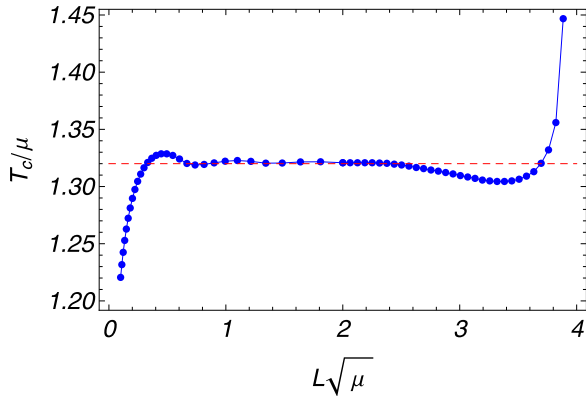

FIG. 6. Dimensional crossover of the superfluid critical temperature T_c for a fixed value of a_{2D}. We use the parameters described in Appendix A. One observes three characteristic regimes for the behavior of the critical temperature: (i) For small $0.1 \leqslant L\sqrt{\mu} \leqslant 1$, the transition temperature increases. However, since we have chosen $\Lambda/\sqrt{\mu} = 10$ here, this region corresponds to $1 \leqslant L\Lambda \leqslant 10$ and thus violates the criterion $L \gg \Lambda^{-1}$. Thus it is not of relevance for this discussion. (ii) For intermediate $L\sqrt{\mu}$, the critical temperature settles at $T_c/\mu = 1.32$ (dashed horizontal line), which is the transition temperature for the corresponding 2D gas with the same value of a_{2D}. In this region, which corresponds to $L/a_{2D} = (1-3) \times 10^3$ in this particular case, the gas is truly two-dimensional. (iii) For larger L, we find an *increase* in the critical temperature. Note that the crossover scale $L\sqrt{\mu} \approx 3$ between the 2D and the quasi-2D regime is still much larger than $T^{-1/2}$ and $\mu^{-1/2}$. The slight dimple in T_c/μ before the rise seems to be rooted in the same oscillatory crossover behavior as found for small L, and we do not attribute any deep physical meaning to it at this point.

APPENDIX B: FLOW EQUATIONS

In this Appendix we derive the flow equation for the Bose gas in the dimensional crossover within the derivative expansion for the effective action. In this approach, the kinetic energy of spatial excitations is approximated by a dispersion relation,

$$E_{\vec{q}} = \frac{1}{\bar{Z}(k)}\big[A(k)(q_1^2 + \cdots + q_D^2) + A_z(k)q_{D+1}^2\big], \quad \text{(B1)}$$

with k-dependent running couplings $\bar{Z}(k)$, $A(k)$, and $A_z(k)$. The distinction between A and A_z is subleading for the physics under consideration, as can be understood as follows: For large k we have $A(k) = A_z(k)$ and the dispersion is effectively isotropic. Deviations between A_z and A appear for $k \lesssim L^{-1}$. In this regime, however, excitations with nonzero $q_{D+1}^2 = k_n^2 = (\frac{2\pi n}{L})^2 > 0$ are disfavored by an energetic penalty $\sim L^{-2}$. Accordingly, as long as the prefactor A_z remains of order unity (i.e., it does not become exceptionally small), transverse excitations $\sim A_z k_n^2$ decouple from the RG flow, and the precise value of the prefactor A_z is unimportant.

In the following we first derive the flow equations for the isotropic case with $A = A_z$. This approximation is applied throughout the text. Afterwards we consider the more involved anisotropic case with $A \neq A_z$. We explicitly show that this distinction is unimportant for the observables considered here. In particular, as shown in Fig. 7, the ratio $\xi = A_z/A$ remains of order unity, thus validating the above argument.

1. Isotropic derivative expansion

Our ansatz for the effective average action is given by a derivative expansion,

$$\Gamma_k[\bar{\phi}^*, \bar{\phi}] = \int_X [\bar{\phi}^*(\bar{Z}_k \partial_\tau - A_k \nabla^2)\bar{\phi} + \bar{U}_k(\bar{\phi}^*\bar{\phi})]. \quad \text{(B2)}$$

By introducing renormalized fields $\phi = A_k^{1/2}\bar{\phi}$ we can express the effective average action as

$$\Gamma_k[\phi^*, \phi] = \int_X (\phi^*(Z_k \partial_\tau - \nabla^2)\phi + U_k(\phi^*\phi)) \quad \text{(B3)}$$

with wave-function renormalization $Z_k = \bar{Z}_k/A_k$ [see Eq. (7)] and the effective average potential $U_k(\rho) = \bar{U}_k(\bar{\rho})$. For a detailed discussion of obtaining the projected flow equations for $\bar{Z}_k$, A_k, and $\bar{U}_k$ from the functional flow equation in Eq. (B2), see Appendixes A–C in Ref. [78].

The flow equation for the effective potential is given by

$$\dot{U}_k(\bar{\rho}) = \frac{1}{2}\text{tr}\int_Q \bar{G}_k(Q)\dot{R}_k(Q) \quad \text{(B4)}$$

with the regularized propagator

$$\bar{G}_k(Q) = \frac{1}{\det_Q}\begin{pmatrix} p^q + \bar{U}' & \bar{Z}_k q_0 \\ -\bar{Z}_k q_0 & p^q + \bar{U}' + 2\bar{\rho}\bar{U}'' \end{pmatrix}, \quad \text{(B5)}$$

where $Q = (q_0, \vec{q}, k_n)$, $\vec{q} = (q_1, \ldots, q_D)$ denotes the momentum vector in the noncompact dimensions of space, and k_n the component of the discrete momentum modes due to the transverse confinement. Below we specialize to the case where

Therefore, we have

$$\int_Q = T \sum_{\omega_n} \frac{1}{L} \sum_{k_n} \int \frac{d^D q}{(2\pi)^D}. \quad \text{(B10)}$$

The flow equation for the effective potential can be written in the form

$$
\begin{aligned}
\dot{U}_k &= \int_Q \frac{p^q + \bar{U}' + \bar{\rho}\bar{U}''}{\det_Q} \dot{R}_k \\
&= T \sum_{\omega_n} \frac{1}{L} \sum_{k_n} 4 v_D \int_0^\infty dq\, q^{D-1} \frac{p^q + \bar{U}' + \bar{\rho}\bar{U}''}{\det_Q} \\
&\quad \times A_k \big(2k^2 - \eta(k^2 - q^2 - k_n^2)\big) \theta\big(k^2 - q^2 - k_n^2\big).
\end{aligned}
\quad \text{(B11)}
$$

Here we have already performed the angular integration of the D-dimensional integral, which gives a factor of $4 v_D = [2^{D-1} \pi^{D/2} \Gamma(D/2)]^{-1}$. The overall θ function limits the integration to the region $q < \sqrt{k^2 - k_n^2}$ and we may replace $p^q \to A_k k^2$ in the integrand. We switch to renormalized quantities $Z_k = \bar{Z}_k / A_k$ and $\rho = A_k \bar{\rho}$ and find

$$
\begin{aligned}
\dot{U}_k &= 4 v_D \left[T \sum_{\omega_n} \frac{k^2 + U' + \rho U''}{(k^2 + U')(k^2 + U' + 2\rho U'') + (Z_k \omega_n)^2} \right] \\
&\quad \times \frac{1}{L} \sum_{k_n} \int_0^{\sqrt{k^2 - k_n^2}} dq\, q^{D-1} \big[2k^2 - \eta(k^2 - q^2 - k_n^2)\big] \\
&\quad \times \theta\big(k^2 - q^2 - k_n^2\big).
\end{aligned}
\quad \text{(B12)}
$$

For the q integration we obtain analytically

$$
\begin{aligned}
&\int_0^{\sqrt{k^2 - k_n^2}} dq\, q^{D-1} \big[2k^2 - \eta(k^2 - q^2 - k_n^2)\big] \theta\big(k^2 - q^2 - k_n^2\big) \\
&= \frac{2}{D} k^{2+D} [1 - (k_n/k)^2]^{D/2} \left[1 - \eta \frac{1 - (k_n/k)^2}{D+2}\right] \theta\big(k^2 - k_n^2\big).
\end{aligned}
\quad \text{(B13)}
$$

The temperature-dependent part evaluates to

$$
\begin{aligned}
&T \sum_{\omega_n} \frac{k^2 + U' + \rho U''}{(k^2 + U')(k^2 + U' + 2\rho U'') + (Z_k \omega_n)^2} \\
&= \frac{1}{2 Z_k} \left(\sqrt{\frac{1 + w_1}{1 + w_2}} + \sqrt{\frac{1 + w_2}{1 + w_1}} \right) \\
&\quad \times \left[\frac{1}{2} + N_B \left(\frac{k^2 \sqrt{(1 + w_1)(1 + w_2)}}{Z_k} \right) \right],
\end{aligned}
\quad \text{(B14)}
$$

where we have introduced the dimensionless quantities $w_1 = U'/k^2$, $w_2 = (U' + 2\rho U'')/k^2$ and the Bose function $N_B(x) = (e^{x/T} - 1)^{-1}$. The flow for the effective potential therefore reads

$$\dot{U}_k = \frac{4 v_D k^{3+D}}{D Z_k} G_1(T) F(\tilde{L}),$$

$$G_1(T) = \left(\sqrt{\frac{1 + w_1}{1 + w_2}} + \sqrt{\frac{1 + w_2}{1 + w_1}} \right) \left(\frac{1}{2} + N_B \right),$$
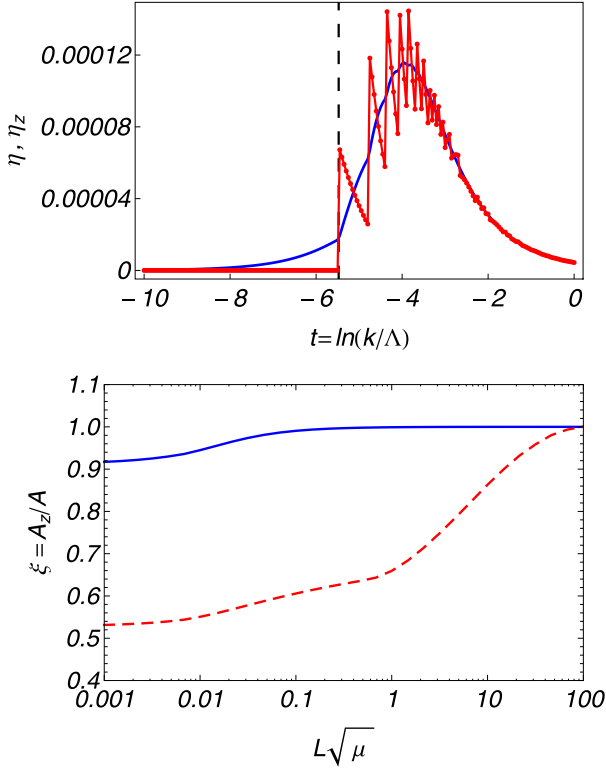

FIG. 7. Top: Characteristic scale dependence of η and η_z within the anisotropic derivative expansion. Whereas the planar anomalous dimension η (blue curve) remains continuous, the transverse anomalous dimension η_z has discontinuous jumps due to the successive integration of modes and the step function in the regulator, Eq. (B40). The function $\eta_z(k)$ follows the behavior of $\eta(k)$ on average for $k > \frac{2\pi}{L}$ and vanishes below $k = \frac{2\pi}{L}$ (shown as the dashed vertical line). The plot is shown for $T = 0$, $L\sqrt{\mu} = 15$, $g_{3D}\sqrt{\mu} = 0.025$. The qualitative behavior of η and η_z is independent of this choice. Bottom: Ratio $\xi = A_z/A$ at the lowest momentum k_f with parameters as in Fig. 4 for zero temperature (upper, blue curve) and at T_c (lower, red curve). Since ξ is of order unity—and not exceptionally small—the isotropic derivative expansion is sufficient to compute observables like the critical temperature.

$D = 2$. Further,

$$\det_Q = (p^q + \bar{U}' + 2\bar{\rho}\bar{U}'')(p^q + \bar{U}') + (\bar{Z}_k q_0)^2, \quad \text{(B6)}$$

$$p^q = A_k(\vec{q}^2 + k_n^2) + R_k(Q), \quad \text{(B7)}$$

where a prime denotes a derivative with respect to $\bar{\rho}$ and an over dot denotes $\partial_t = k \partial_k$. In this calculation we use the Litim-type regulator [23,79,80]

$$R_k(Q) = A_k(k^2 - \vec{q}^2 - k_n^2)\theta(k^2 - \vec{q}^2 - k_n^2), \quad \text{(B8)}$$

$$\dot{R}_k(Q) = A_k[2k^2 - \eta(k^2 - \vec{q}^2 - k_n^2)]\theta(k^2 - \vec{q}^2 - k_n^2), \quad \text{(B9)}$$

where we define the anomalous dimension by $\eta = -\dot{A}_k/A_k$. The integration in Eq. (B4) consists of a q_0 integral, which is replaced by a sum over Matsubara frequencies ω_n for nonzero temperatures and an integration over spatial dimensions.

$$F(\tilde{L}) = \frac{1}{Lk} \sum_{k_n} [1 - (k_n/k)^2]^{D/2}$$

$$\times \left(1 - \eta \frac{1 - (k_n/k)^2}{D+2}\right)\theta\left(k^2 - k_n^2\right) \quad \text{(B15)}$$

with $\tilde{L} = Lk$.

We now specialize to two continuous dimensions. Further, we compactify on a torus, thus $k_n = 2\pi n/L$, $n \in \mathbb{Z}$. The θ function limits the range of summation in the crossover function to $|k_n| = |\frac{2\pi}{L}n| < k$ or, equivalently, $|n| < \frac{\tilde{L}}{2\pi}$. With $N = \lfloor \frac{\tilde{L}}{2\pi} \rfloor$ we can write

$$F_{\text{pbc}}(\tilde{L}) = \frac{1}{\tilde{L}}\left[\left(1 - \frac{\eta}{4}\right)\sum_{n=-N}^{n=N} 1\right.$$

$$\left. - \left(1 - \frac{\eta}{2}\right)\sum_{n=-N}^{n=N} \frac{k_n^2}{k^2} - \frac{\eta}{4}\sum_{n=-N}^{n=N} \frac{k_n^4}{k^4}\right]. \quad \text{(B16)}$$

Together with

$$\sum_{n=-N}^{N} \frac{k_n^2}{k^2} = 2\left(\frac{2\pi}{\tilde{L}}\right)^2 \sum_{n=1}^{N} n^2,$$

$$\sum_{n=-N}^{N} \frac{k_n^4}{k^4} = 2\left(\frac{2\pi}{\tilde{L}}\right)^4 \sum_{n=1}^{N} n^4 \quad \text{(B17)}$$

and

$$\sum_{n=-N}^{n=N} 1 = 1 + 2N,$$

$$\sum_{n=1}^{N} n^2 = \frac{1}{6}N(1+N)(1+2N), \quad \text{(B18)}$$

$$\sum_{n=1}^{N} n^4 = \frac{1}{30}N(1+N)(1+2N)(-1+3N+3N^2),$$

the crossover function evaluates to

$$F_{\text{pbc}}(\tilde{L}) = \frac{2N+1}{\tilde{L}}\left[1 - \frac{\eta}{4} - \frac{1}{\tilde{L}^2}\left(1 - \frac{\eta}{2}\right)\frac{4\pi^2}{3}N(N+1)\right.$$

$$\left. - \frac{\eta}{\tilde{L}^4}\frac{4\pi^4}{15}N(N+1)(-1+3N+3N^2)\right]. \quad \text{(B19)}$$

The flow for the effective potential with $v_2 = 1/8\pi$ and $\dot{U}_k = \dot{U}_k + \eta\rho U'_k$ reads

$$\dot{U}_k = \eta\rho U'_k + \frac{k^5}{4\pi Z_k}G_1(T)F(\tilde{L}). \quad \text{(B20)}$$

We use the derivative projection to obtain the flow equations for the wave-function renormalizations $\bar{Z}_k$ and A_k defined via

$$\partial_t \bar{Z}_k = -\frac{\partial}{\partial p_0}\dot{G}^{-1}_{k,12}(p_0,0)\bigg|_{p_0=0},$$

$$\partial_t A_k = \frac{\partial}{\partial p^2}\dot{G}^{-1}_{k,22}(0,p^2)\bigg|_{p=0}, \quad \text{(B21)}$$

where $G^{-1}_{k,ij}(p_0,p^2) = \delta^2\Gamma/(\delta\phi_i\delta\phi_j)|_{\rho_0}$ denotes the second functional derivative. For the flow of $\bar{Z}_k$ we arrive at

$$\bar{Z}_k^{-1}\partial_t\bar{Z}_k = 4\rho U''^2 \int_Q \frac{k^4 - 2\rho U''(k^2 + \rho U'') + (Z_k q_0)^2}{(k^2(k^2 + 2\rho U'') + (Z_k q_0)^2)^3}$$

$$\times [2k^2 - \eta(k^2 - q^2 - k_n^2)]\theta(k^2 - q^2 - k_n^2). \quad \text{(B22)}$$

Again, we can evaluate

$$\frac{1}{L}\sum_{k_n}\int \frac{d^D q}{(2\pi)^D}\left(2k^2 - \eta(k^2 - q^2 - k_n^2)\right)\theta(k^2 - q^2 - k_n^2)$$

$$= 4v_D \frac{2}{D}k^{3+D}F(\tilde{L}), \quad \text{(B23)}$$

with $F(\tilde{L})$ as defined in Eq. (B15). Together with $U'' = \lambda$ and $\bar{Z}_k = Z_k A_k$, we obtain

$$\partial_t Z_k = \eta Z_k - Z_k 4\rho\lambda^2 \frac{8v_D k^{3+D}}{D}\frac{1}{2Z_k k^6}G_2(T)F(\tilde{L}), \quad \text{(B24)}$$

where we have defined the temperature-dependent function

$$G_2(T) = \frac{1}{(1+w_2)^{3/2}}\left(\frac{1}{2} + N_B(c) - cN'_B(c)\right)$$

$$- \frac{3}{8}\frac{w_2(4+w_2)}{(1+w_2)^{5/2}}$$

$$\times \left(\frac{1}{2} + N_B(c) - cN'_B(c) + \frac{c^2}{3}N''_B(c)\right), \quad \text{(B25)}$$

with $c = k^2\sqrt{1+w_2}/Z_k$ and $N_B(c) = (e^{c/T} - 1)^{-1}$. Specifying to $D = 2$ noncompact dimensions we arrive at

$$\partial_t Z_k = \eta Z_k - \frac{\rho\lambda^2}{\pi k}G_2(T)F(\tilde{L}). \quad \text{(B26)}$$

For the flow equation for A_k we need to take a derivative with respect to $|\vec{p}|^2$. We consider the external momentum as a 2D vector $\vec{p} = (p_x, p_y)$. We then have, with $x = (\vec{q}\cdot\vec{p})/(qp)$ and $\eta = -(\partial_t A_k)/A_k$,

$$\eta = 8\rho\lambda^2\left(T\sum_{\omega_n}\frac{1}{\det^2_Q}\right)\frac{1}{L}\sum_{k_n}\int \frac{d^2 q}{(2\pi)^2}q^2 x^2\delta(k^2 - q^2 - k_n^2)$$

$$\times \left(2k^2 - \eta(k^2 - q^2 - k_n^2)\right)\theta(k^2 - q^2 - k_n^2). \quad \text{(B27)}$$

Angle integration over x yields another factor of $1/2$. We have

$$\eta = 8\rho\lambda^2\left(T\sum_{\omega_n}\frac{1}{\det^2_Q}\right)\frac{1}{L}\sum_{k_n}4v_2\frac{1}{2}\int dq\, q^2$$

$$\times \left(2k^2 - \eta(k^2 - q^2 - k_n^2)\right)\delta(k^2 - q^2 - k_n^2)$$

$$\times \theta(k^2 - q^2 - k_n^2). \quad \text{(B28)}$$

We further obtain

$$\eta = \frac{32\rho\lambda^2 v_2}{2}\left(T\sum_{\omega_n}\frac{1}{\det^2_Q}\right)\frac{1}{L}\sum_{k_n}$$

$$\times \frac{1}{2}\int dq\, q^3\left(2k^2 - \eta(k^2 - q^2 - k_n^2)\right)\delta(k^2 - q^2 - k_n^2). \quad \text{(B29)}$$

By reformulating the δ function,

$$
\delta\big(k^2 - k_n^2 - q^2\big)
$$
$$
= \frac{1}{2\sqrt{k^2 - k_n^2}}\big[\delta\big(\sqrt{k^2 - k_n^2} - q\big) + \delta\big(\sqrt{k^2 - k_n^2} + q\big)\big],
$$
(B30)

and using that the second δ function gives no contribution to the integral, we get

$$
\eta = \frac{32\rho\lambda^2 v_2}{2}\Bigg(T\sum_{\omega_n}\frac{1}{\det_Q^2}\Bigg)\frac{1}{L}\sum_{k_n}
$$
$$
\times \frac{1}{2}\frac{1}{2}\big(k^2 - k_n^2\big)^{-1/2}\big(k^2 - k_n^2\big)^{3/2}2k^2
$$
$$
= \frac{32\rho\lambda^2 v_2}{2}\Bigg(T\sum_{\omega_n}\frac{1}{\det_Q^2}\Bigg)\frac{1}{L}\sum_{k_n}\frac{1}{2}k^2\big(k^2 - k_n^2\big). \quad (B31)
$$

We find

$$
\eta = \frac{32\rho\lambda^2}{32\pi}\Bigg(T\sum_{\omega_n}\frac{1}{\det_Q^2}\Bigg)\frac{k^4}{L}\sum_{k_n}[1 - (k_n/k)^2]. \quad (B32)
$$

And finally,

$$
\eta = \frac{\rho\lambda^2}{\pi}k^5\Bigg(T\sum_{\omega_n}\frac{1}{\det_Q^2}\Bigg)\frac{1}{\tilde{L}}\sum_{k_n}(1 - (k_n/k)^2)
$$
$$
= \frac{\rho\lambda^2}{\pi}k^5\Bigg(T\sum_{\omega_n}\frac{1}{\det_Q^2}\Bigg)F_0(\tilde{L}), \quad (B33)
$$

where $F_0(\tilde{L})$ is the crossover function with η set equal to 0, i.e.,

$$
F_0(\tilde{L}) = \frac{2N + 1}{\tilde{L}}\Bigg[1 - \frac{1}{\tilde{L}^2}\frac{4\pi^2}{3}N(N + 1)\Bigg]. \quad (B34)
$$

The Matsubara summation yields

$$
T\sum_{\omega_n}\frac{1}{\det_Q^2} = \frac{1}{2Z_k k^6}G_3(T), \quad (B35)
$$

with

$$
G_3(T) = \frac{1}{(1 + w_2)^{3/2}}\Big(\frac{1}{2} + N_B(c) - cN_B'(c)\Big), \quad (B36)
$$

with $c = k^2(1 + w_2)^{1/2}/Z_k$ and $N_B(c) = (e^{c/T} - 1)^{-1}$ as before. The anomalous dimension then reads

$$
\eta = \frac{\rho_0\lambda^2}{2\pi Z_k k}G_3(T)F_0(\tilde{L}). \quad (B37)
$$

This completes the derivation of the flow equations.

2. Anisotropic derivative expansion

In the following we consider the anisotropic extension of Eq. (B2) given by

$$
\Gamma_k[\bar{\phi}^*, \bar{\phi}] = \int_X \big[\bar{\phi}^*\big(\bar{Z}\partial_\tau - A\nabla^2 - A_z\partial_z^2\big)\bar{\phi} + \bar{U}(\bar{\phi}^*\bar{\phi})\big],
$$
(B38)

with $\nabla^2 = \partial_x^2 + \partial_y^2$. For concreteness we restrict ourselves to the crossover from three to two dimensions in this section, and the k dependence of running couplings is understood implicitly. We write

$$
\xi = \frac{A_z}{A}, \quad \eta_z = -\frac{\dot{A}_z}{A}. \quad (B39)
$$

The isotropic case corresponds to $\xi = 1$ and $\eta = \eta_z$. Due to $A_\Lambda = A_{z,\Lambda} = 1$ this implies $A = A_z$ for all k. This behavior is recovered in the anisotropic parametrization for large k. The infrared regulator function is chosen to be

$$
R_k(Q) = A\big(k^2 - q^2 - \xi q_z^2\big)\theta\big(k^2 - q^2 - \xi q_z^2\big) \quad (B40)
$$

with $q^2 = \vec{q}^2 = q_x^2 + q_y^2$. The regulator is designed such that the usual replacement $p^q \to Ak^2$ in the integrand is applicable.

The derivation of the flow equations for $\bar{U}$, A, A_z, and $\bar{Z}$ is analogous to the isotropic case so that we limit the presentation to a few central statements. The β functions for the effective potential $\bar{U}$ and frequency coefficient $\bar{Z}$ in Eqs. (B20) and (B24), respectively, need to be equipped with the modified crossover function

$$
F_{\mathrm{pbc}}(\tilde{L}) = \frac{2N + 1}{\tilde{L}}\Bigg[1 - \frac{\eta}{4} - \frac{1}{\tilde{L}^2}\Big(\xi - \frac{\eta}{2}\Big)\frac{4\pi^2}{3}N(N + 1)
$$
$$
- \frac{\xi(2\eta_z - \xi\eta)}{\tilde{L}^4}\frac{4\pi^4}{15}N(N + 1)(-1 + 3N + 3N^2)\Bigg]
$$
(B41)

instead of Eq. (B19). For the projection of the flow equations for A and A_z, respectively, we employ

$$
\dot{A} = \frac{\partial}{\partial p^2}\dot{G}_{k,22}^{-1}(0, \vec{p}^2 = p^2, p_z = 0)\Big|_{P=0}, \quad (B42)
$$
$$
\dot{A}_z = \frac{\partial}{\partial p_z^2}\dot{G}_{k,22}^{-1}(0, \vec{p}^2 = 0, p_z)\Big|_{P=0}. \quad (B43)
$$

Although q_z is not a continuous variable for $L < \infty$, this is the natural generalization of the appropriate infinite volume projection; see also the definition of $\dot{Z}$ from Eq. (B21). For the anomalous dimensions η and η_z we obtain

$$
\begin{Bmatrix}\eta \\ \eta_z\end{Bmatrix} = 8\rho_0\lambda^2\int_Q\frac{1}{\det_Q^2}\big[(2 - \eta)k^2 + \eta q^2 + \eta_z q_z^2\big]
$$
$$
\times\begin{Bmatrix}\frac{1}{D}q^2 \\ \xi^2 q_z^2\end{Bmatrix}\delta\big(k^2 - q^2 - \xi q_z^2\big)\theta\big(k^2 - q^2 - \xi q_z^2\big).
$$
(B44)

For $\tilde{L} = \infty$ we can employ $\int_Q q_z^2 = \frac{1}{D}\int_Q q^2$ such that $\eta = \eta_z$ and $\xi = 1$ is a consistent solution. For $\tilde{L} < \infty$, Eq. (B44) lead to a linear set of equations for η and η_z, which supplements the remaining flow equations. The flow of the running coupling ξ is given by

$$
\dot{\xi} = \eta\xi - \eta_z. \quad (B45)
$$

From the solution of the RG flow in the anisotropic derivative expansion we find the following features: (i) The anomalous dimension η_z follows the behavior of η for $k > \frac{2\pi}{L}$ on average, though in a discontinuous manner. For $k \leqslant \frac{2\pi}{L}$,

η_z vanishes, whereas η remains nonzero. This behavior is displayed in the upper panel in Fig. 7. (ii) The value of $\xi = A_z/A$ at $k = k_f$ remains of order unity. It is close to $\xi = 1$ at zero temperature, whereas it is in the range $\xi \simeq 0.5$–1 at T_c (see lower panel in Fig. 7). (iii) The extracted critical temperature T_c as a function of L and g_{3D} is identical to that of the isotropic derivative expansion within the resolution of Fig. 4. This good agreement can be understood from the fact that η_z closely follows the behavior of η, but η itself is small. Hence the influence of η on T_c is already a subleading effect, such that the difference between η and η_z is only a second-order subleading effect.

The good agreement of results within the anisotropic versus isotropic derivative expansions justify the use of the isotropic parametrization with $A_z = A$ for the computation of observables in the text.

APPENDIX C: T-MATRIX, SCATTERING VERTEX, AND DIMER PROPAGATOR

In this Appendix we clarify the roles played by the low-energy T matrix, the scattering vertex, and the dimer propagator in the FRG approach to scattering of nonrelativistic bosons. A key result for the analysis of the dimensional crossover is given by the translation formulas between the initial couplings λ_Λ of the RG flow and the scattering lengths a. In this section we denote the 2D and 3D scattering lengths a_3 and a_2, respectively. We further write

$$\mathcal{P}_\phi(Q) = \mathcal{P}_\phi^Q = iq_0 + q^2 - \mu \qquad \text{(C1)}$$

for the inverse atom propagator with $\mu \leqslant 0$. The temperature is set to $T = 0$ for the scattering problem.

1. T matrix

The T matrix from Eq. (46) can be defined more generally as a function of $P = (p_0, \vec{p})$ by

$$\frac{1}{T(P)} = \frac{1}{\lambda_\Lambda^{(sh)}} + \int_Q^\Lambda \frac{1}{\mathcal{P}_\phi(Q+P)\mathcal{P}_\phi(-Q)}. \qquad \text{(C2)}$$

The UV cutoff Λ only restricts the spatial momenta. Performing the loop integration we obtain

$$\frac{1}{T(P)} = \begin{cases} \frac{1}{\lambda_{3D,\Lambda}^{(sh)}} + \frac{\Lambda}{4\pi^2} - \frac{1}{8\pi}\sqrt{A} & (D=3), \\ \frac{1}{\lambda_{2D,\Lambda}^{(sh)}} - \frac{1}{8\pi}\ln(A/\Lambda^2) & (D=2), \end{cases} \qquad \text{(C3)}$$

with

$$A = \frac{ip_0}{2} + \frac{p^2}{4} - \mu. \qquad \text{(C4)}$$

The analytic continuation to real frequencies (energies) E is given by $ip_0 \rightarrow -(E + i0)$. This yields the low-energy T matrix $T(E)$ provided we further choose $p^2 = \mu = 0$. To summarize, we obtain the T matrix $T(E)$ by replacing

$$A \rightarrow -\frac{E + i0}{2}. \qquad \text{(C5)}$$

2. Scattering vertex

By relating the running coupling constant λ_k to the T matrix we are able to define a_3 and a_2 within the FRG setup. The flow equation for λ_k in vacuum ($\mu = T = 0$) is found from $\dot{\lambda}_k = \dot{U}''(0)$, where

$$\dot{U}(\rho) = \frac{1}{2}\int_Q \dot{R}_k(Q)\frac{L_\phi^Q + L_\phi^{-Q}}{L_\phi^Q L_\phi^{-Q} - (\rho U'')^2} \qquad \text{(C6)}$$

and $L_\phi^Q = \mathcal{P}_\phi(Q) + R_k(Q) + U' + \rho U''$. Hence

$$\begin{aligned} \dot{\lambda}_k &= 2\lambda_k^2 \int_Q \frac{\dot{R}_k(Q)}{(\mathcal{P}_\phi^Q + R_k^Q)^2(\mathcal{P}_\phi^{-Q} + R_k^{-Q})} \\ &= -\lambda_k^2 \partial_t \int_Q \frac{1}{(\mathcal{P}_\phi^Q + R_k^Q)(\mathcal{P}_\phi^{-Q} + R_k^{-Q})}. \end{aligned} \qquad \text{(C7)}$$

We conclude that

$$\partial_t \frac{1}{\lambda_k} = \partial_t \int_Q \frac{1}{(\mathcal{P}_\phi^Q + R_k^Q)(\mathcal{P}_\phi^{-Q} + R_k^{-Q})}, \qquad \text{(C8)}$$

which is readily solved by

$$\begin{aligned} \frac{1}{\lambda_k} &= \frac{1}{\lambda_\Lambda} + \int_Q \left(\frac{1}{(\mathcal{P}_\phi^Q + R_k^Q)(\mathcal{P}_\phi^{-Q} + R_k^{-Q})} \right. \\ &\quad \left. - \frac{1}{(\mathcal{P}_\phi^Q + R_\Lambda^Q)(\mathcal{P}_\phi^{-Q} + R_\Lambda^{-Q})} \right) \\ &= \frac{1}{\lambda_\Lambda} + \frac{1}{2}\int_{\vec{q}} \left(\frac{1}{q^2 + R_k(q)} - \frac{1}{q^2 + R_\Lambda(q)} \right) \\ &\stackrel{(C10)}{=} \frac{1}{\lambda_\Lambda} + \frac{1}{2}\int_{\vec{q}}^\Lambda \frac{1}{q^2 + R_k(q)} - \frac{1}{2}\int_{\vec{q}}^\Lambda \frac{1}{\Lambda^2}. \end{aligned} \qquad \text{(C9)}$$

In the last line we have employed the particular form of the Litim-type regulator given by

$$R_k(q) = (k^2 - q^2)\theta(k^2 - q^2). \qquad \text{(C10)}$$

For the last term in Eq. (C9) we find

$$\frac{1}{2}\int_{\vec{q}}^\Lambda \frac{1}{\Lambda^2} = \begin{cases} \frac{\Lambda}{12\pi^2} & (D=3), \\ \frac{1}{8\pi} & (D=2). \end{cases} \qquad \text{(C11)}$$

We generalize this to a P-dependent scattering vertex by defining

$$\partial_t \frac{1}{\lambda_k(P)} := \partial_t \int_Q \frac{1}{(\mathcal{P}_\phi^{Q+P} + R_k^{Q+P})(\mathcal{P}_\phi^{-Q} + R_k^{-Q})}. \qquad \text{(C12)}$$

For nonzero P we can take the limit $k \rightarrow 0$ and find

$$\frac{1}{\lambda_{k=0}(P)} = \frac{1}{\lambda_\Lambda} + \int_Q^\Lambda \frac{1}{\mathcal{P}_\phi^{Q+P}\mathcal{P}_\phi^{-Q}} - \frac{1}{2}\int_{\vec{q}}^\Lambda \frac{1}{\Lambda^2}$$

due to $R_{k=0} = 0$. Comparing this to Eq. (C2) for the T matrix $T(P)$ we conclude that

$$T(P) = \lambda_{k=0}(P). \qquad \text{(C13)}$$

For the renormalization of the coupling constants we have

$$\frac{1}{\lambda_\Lambda^{(sh)}} = \frac{1}{\lambda_\Lambda} - \frac{1}{2}\int_{\vec{q}}^\Lambda \frac{1}{\Lambda^2}. \qquad \text{(C14)}$$

The additional term on the right-hand side results from the particular form of the regulator (C10) employed in our FRG approach. As a consequence, the relationship between λ_Λ and the scattering length a in the FRG approach is given by

$$\frac{1}{\lambda_\Lambda^{3D}} = -\frac{\Lambda}{6\pi^2} + \frac{1}{8\pi a_3}, \tag{C15}$$

$$\frac{1}{\lambda_\Lambda^{2D}} = -\frac{1}{8\pi} \ln\left(\Lambda^2 a_2^2\right) + \frac{1}{8\pi}. \tag{C16}$$

3. Dimer propagator

The scattering vertex $\lambda_k(P)$ has an intuitive interpretation in terms of the inverse dimer propagator

$$\mathcal{P}_{dim}(P) := -\frac{1}{\lambda_{k=0}(P)} = -\frac{1}{T(P)}, \tag{C17}$$

which describes interactions between atoms by means of a propagating dimer boson with frequency and momentum P. Within the sharp momentum cutoff scheme we have

$$\mathcal{P}_{dim}(P) = -\frac{1}{\lambda_\Lambda^{(sh)}} - \int_Q^\Lambda \frac{1}{\mathcal{P}_\phi(Q+P)\mathcal{P}_\phi(-Q)}. \tag{C18}$$

Due to Galilean invariance, the P dependence of the dimer propagator is solely in terms of

$$A = \frac{1}{2}\left(ip_0 + \frac{p^2}{2} - 2\mu\right), \tag{C19}$$

which reflects the dimer mass and dimer chemical potential being $M_{dim} = 2M$ and $\mu_{dim} = 2\mu$, respectively.

[1] I. Bloch, J. Dalibard, and W. Zwerger, Rev. Mod. Phys. **80**, 885 (2008).

[2] M. Lewenstein, A. Sanpera, V. Ahufinger, B. Damski, A. Sen(De), and U. Sen, Adv. Phys. **56**, 243 (2007).

[3] Z. Hadzibabic, P. Krüger, M. Cheneau, B. Battelier, and J. Dalibard, Nature **441**, 1118 (2006).

[4] P. Cladé, C. Ryu, A. Ramanathan, K. Helmerson, and W. D. Phillips, Phys. Rev. Lett. **102**, 170401 (2009).

[5] S. Tung, G. Lamporesi, D. Lobser, L. Xia, and E. A. Cornell, Phys. Rev. Lett. **105**, 230408 (2010).

[6] T. Plisson, B. Allard, M. Holzmann, G. Salomon, A. Aspect, P. Bouyer, and T. Bourdel, Phys. Rev. A **84**, 061606 (2011).

[7] R. Desbuquois, L. Chomaz, T. Yefsah, J. Léonard, J. Beugnon, C. Weitenberg, and J. Dalibard, Nat. Phys. **8**, 645 (2012).

[8] R. J. Fletcher, M. Robert-de-Saint-Vincent, J. Man, N. Navon, R. P. Smith, K. G. H. Viebahn, and Z. Hadzibabic, Phys. Rev. Lett. **114**, 255302 (2015).

[9] M. G. Ries, A. N. Wenz, G. Zürn, L. Bayha, I. Boettcher, D. Kedar, P. A. Murthy, M. Neidig, T. Lompe, and S. Jochim, Phys. Rev. Lett. **114**, 230401 (2015).

[10] P. A. Murthy, I. Boettcher, L. Bayha, M. Holzmann, D. Kedar, M. Neidig, M. G. Ries, A. N. Wenz, G. Zürn, and S. Jochim, Phys. Rev. Lett. **115**, 010401 (2015).

[11] C. Wetterich, Nucl. Phys. B **352**, 529 (1991).

[12] C. Wetterich, Phys. Lett. B **301**, 90 (1993).

[13] J. Berges, N. Tetradis, and C. Wetterich, Phys. Rep. **363**, 223 (2002).

[14] J. M. Pawlowski, Ann. Phys. **322**, 2831 (2007).

[15] H. Gies, Lect. Notes Phys. **852**, 287 (2012).

[16] B.-J. Schaefer and J. Wambach, Phys. Part. Nucl. **39**, 1025 (2008).

[17] B. Delamotte, Lect. Notes Phys. **852**, 49 (2012).

[18] P. Kopietz, L. Bartosch, and F. Schütz, *Introduction to the Functional Renormalization Group* (Springer, Berlin, 2010).

[19] W. Metzner, M. Salmhofer, C. Honerkamp, V. Meden, and K. Schonhammer, Rev. Mod. Phys. **84**, 299 (2012).

[20] J. Braun, J. Phys. G **39**, 033001 (2012).

[21] I. Boettcher, J. M. Pawlowski, and S. Diehl, Nucl. Phys. Proc. Suppl. **228**, 63 (2012).

[22] J. M. Pawlowski, M. M. Scherer, R. Schmidt, and S. J. Wetzel, arXiv:1512.03598.

[23] C. Wetterich, Phys. Rev. B **77**, 064504 (2008).

[24] S. Floerchinger and C. Wetterich, Phys. Rev. A **77**, 053603 (2008).

[25] S. Floerchinger and C. Wetterich, Phys. Rev. A **79**, 013601 (2009).

[26] N. D. Mermin and H. Wagner, Phys. Rev. Lett. **17**, 1133 (1966).

[27] P. C. Hohenberg, Phys. Rev. **158**, 383 (1967).

[28] S. Floerchinger and C. Wetterich, Phys. Rev. A **79**, 063602 (2009).

[29] A. Rançon and N. Dupuis, Phys. Rev. A **85**, 063607 (2012).

[30] N. Tetradis and C. Wetterich, Nucl. Phys. B **422**, 541 (1994).

[31] N. Prokof'ev, O. Ruebenacker, and B. Svistunov, Phys. Rev. Lett. **87**, 270402 (2001).

[32] N. Prokof'ev and B. Svistunov, Phys. Rev. A **66**, 043608 (2002).

[33] M. Holzmann, G. Baym, J.-P. Blaizot, and F. Laloë, Proc. Natl. Acad. Sci. U.S.A. **104**, 1476 (2007).

[34] M. Holzmann and W. Krauth, Phys. Rev. Lett. **100**, 190402 (2008).

[35] C.-L. Hung, X. Zhang, N. Gemelke, and C. Chin, Nature **470**, 236 (2011).

[36] T. Yefsah, R. Desbuquois, L. Chomaz, K. J. Günter, and J. Dalibard, Phys. Rev. Lett. **107**, 130401 (2011).

[37] X. Zhang, C.-L. Hung, S.-K. Tung, and C. Chin, Science **335**, 1070 (2012).

[38] G. v. Gersdorff and C. Wetterich, Phys. Rev. B **64**, 054513 (2001).

[39] N. Dupuis, Phys. Rev. Lett. **102**, 190401 (2009).

[40] P. Jakubczyk, N. Dupuis, and B. Delamotte, Phys. Rev. E **90**, 062105 (2014).

[41] V. L. Berezinskii, Sov. Phys. JETP **32**, 493 (1971).

[42] V. L. Berezinskii, Sov. Phys. JETP **34**, 610 (1972).

[43] J. M. Kosterlitz and D. J. Thouless, J. Phys. C: Solid State Phys. **6**, 1181 (1973).

[44] J. M. Kosterlitz, J. Phys. C: Solid State Phys. **7**, 1046 (1974).

[45] U. A. Khawaja, N. P. Proukakis, J. O. Andersen, M. W. J. Romans, and H. T. C. Stoof, Phys. Rev. A **68**, 043603 (2003).

[46] J. Braun and B. Klein, Eur. Phys. J. C **63**, 443 (2009).

[47] J. Braun, B. Klein, and P. Piasecki, Eur. Phys. J. C **71**, 1576 (2011).

[48] J. Braun, B. Klein, and B.-J. Schaefer, Phys. Lett. B **713**, 216 (2012).

[49] R.-A. Tripolt, J. Braun, B. Klein, and B.-J. Schaefer, Phys. Rev. D **90**, 054012 (2014).

[50] J. Braun, S. Diehl, and M. M. Scherer, Phys. Rev. A **84**, 063616 (2011).

[51] N. Tetradis and C. Wetterich, Nucl. Phys. B **398**, 659 (1993).

[52] N. Tetradis and C. Wetterich, Int. J. Mod. Phys. A **9**, 4029 (1994).

[53] P. Grüter, D. Ceperley, and F. Laloë, Phys. Rev. Lett. **79**, 3549 (1997).

[54] G. Baym, J.-P. Blaizot, M. Holzmann, F. Laloë, and D. Vautherin, Phys. Rev. Lett. **83**, 1703 (1999).

[55] M. Holzmann and W. Krauth, Phys. Rev. Lett. **83**, 2687 (1999).

[56] P. Arnold and G. Moore, Phys. Rev. Lett. **87**, 120401 (2001).

[57] V. A. Kashurnikov, N. V. Prokof'ev, and B. V. Svistunov, Phys. Rev. Lett. **87**, 120402 (2001).

[58] A. M. Fischer and M. M. Parish, Phys. Rev. B **90**, 214503 (2014).

[59] D. S. Petrov and G. V. Shlyapnikov, Phys. Rev. A **64**, 012706 (2001).

[60] J. Levinsen and M. M. Parish, Annu. Rev. Cold At. Mol. **3**, 1 (2015).

[61] S. Floerchinger, Nucl. Phys. A **927**, 119 (2014).

[62] M. T. Yamashita, F. F. Bellotti, T. Frederico, D. V. Fedorov, A. S. Jensen, and N. T. Zinner, J. Phys. B: At. Mol. Phys. **48**, 025302 (2015).

[63] S. A. Morgan, M. D. Lee, and K. Burnett, Phys. Rev. A **65**, 022706 (2002).

[64] K. Sun and C. J. Bolech, Phys. Rev. A **85**, 051607 (2012).

[65] S. Dutta and E. J. Mueller, arXiv:1508.03352.

[66] P. A. Lee, N. Nagaosa, and X.-G. Wen, Rev. Mod. Phys. **78**, 17 (2006).

[67] I. Carusotto and C. Ciuti, Rev. Mod. Phys. **85**, 299 (2013).

[68] L. M. Sieberer, M. Buchhold, and S. Diehl, arXiv:1512.00637 [cond-mat.quant-gas].

[69] J. Berges and D. Mesterhazy, Nucl. Phys. Proc. Suppl. **228**, 37 (2012).

[70] V. Makhalov, K. Martiyanov, and A. Turlapov, Phys. Rev. Lett. **112**, 045301 (2014).

[71] P. Dyke, K. Fenech, T. Peppler, M. G. Lingham, S. Hoinka, W. Zhang, S.-G. Peng, B. Mulkerin, H. Hu, X.-J. Liu, and C. J. Vale, Phys. Rev. A **93**, 011603 (2016).

[72] K. Fenech, P. Dyke, T. Peppler, M. G. Lingham, S. Hoinka, H. Hu, and C. J. Vale, Phys. Rev. Lett. **116**, 045302 (2016).

[73] I. Boettcher, L. Bayha, D. Kedar, P. A. Murthy, M. Neidig, M. G. Ries, A. N. Wenz, G. Zürn, S. Jochim, and T. Enss, Phys. Rev. Lett. **116**, 045303 (2016).

[74] J. N. Fuchs, X. Leyronas, and R. Combescot, Phys. Rev. A **68**, 043610 (2003).

[75] H. Heiselberg, Phys. Rev. Lett. **93**, 040402 (2004).

[76] I. Boettcher, S. Floerchinger, and C. Wetterich, J. Phys. B **44**, 235301 (2011).

[77] R. Schmidt, T. Enss, V. Pietilä, and E. Demler, Phys. Rev. A **85**, 021602 (2012).

[78] I. Boettcher, J. M. Pawlowski, and C. Wetterich, Phys. Rev. A **89**, 053630 (2014).

[79] D. F. Litim, Int. J. Mod. Phys. A **16**, 2081 (2001).

[80] D. F. Litim, Phys. Lett. B **486**, 92 (2000).